FEMS Microbiology Ecology, 2024, **100**, fiae119
DOI: 10.1093/femsec/fiae119
Advance access publication date: 18 September 2024
Research Article

Transient hypoxia drives soil microbial community dynamics and biogeochemistry during human decomposition

Lois S. Taylor [1,*], Allison R. Mason [2], Hannah L. Noel [2], Michael E. Essington [1], Mary C. Davis [3], Veronica A. Brown [2], Dawnie W. Steadman [3], Jennifer M. DeBruyn [1,*]

[1]Department of Biosystems Engineering and Soil Science, University of Tennessee, Knoxville, TN 37996, USA
[2]Department of Microbiology, University of Tennessee, Knoxville, TN 37996, USA
[3]Department of Anthropology, University of Tennessee, Knoxville, TN 37996, USA
*Corresponding authors. Lois S.Taylor, Biosystems Engineering and Soil Science, University of Tennessee, 2506 E.J. Chapman Drive, Knoxville, TN 37996, United States. E-mail: ltaylo32@utk.edu; Jennifer M. DeBruyn, Biosystems Engineering and Soil Science, University of Tennessee, 2506 E.J. Chapman Drive, Knoxville, TN 37996, United States. E-mail: jdebruyn@utk.edu
Editor: [Petr Baldrian]

Abstract

Human decomposition in terrestrial ecosystems is a dynamic process creating localized hot spots of soil microbial activity. Longer-term (beyond a few months) impacts on decomposer microbial communities are poorly characterized and do not typically connect microbial communities to biogeochemistry, limiting our understanding of decomposer communities and their functions. We performed separate year-long human decomposition trials, one starting in spring, another in winter, integrating bacterial and fungal community structure and abundances with soil physicochemistry and biogeochemistry to identify key drivers of microbial community change. In both trials, soil acidification, elevated microbial respiration, and reduced soil oxygen concentrations occurred. Changes in soil oxygen concentrations were the primary driver of microbial succession and nitrogen transformation patterns, while fungal community diversity and abundance was related to soil pH. Relative abundance of facultative anaerobic taxa (*Firmicutes* and *Saccharomycetes*) increased during the period of reduced soil oxygen. The magnitude and timing of the decomposition responses were amplified during the spring trial relative to the winter, even when corrected for thermal inputs (accumulated degree days). Further, soil chemical parameters, microbial community structure, and fungal gene abundances remained altered at the end of 1 year, suggesting longer-term impacts on soil ecosystems beyond the initial pulse of decomposition products.

Keywords: biogeochemical hotspot; forensic taphonomy; human decomposition; necrobiome; soil biogeochemistry; soil microbiology

Introduction

Human decomposition in terrestrial ecosystems is a dynamic process that creates localized hotspots of soil nutrient cycling (Keenan et al. 2018a, b, DeBruyn et al. 2021) and microbial activity (Cobaugh et al. 2015, Metcalf et al. 2016, Adserias-Garriga et al. 2017, Mason et al. 2022). The study of its progression through time and under varied environmental conditions is crucial to our understanding mechanisms involved in recycling cadaver-derived organic matter. From a soil ecological perspective, vertebrate decomposition (both human and animal) results in a spectrum of changes to prevailing soil chemistry and subsequent biogeochemical cycling, as well as affecting the community structure, diversity, and function of microbial decomposer communities inhabiting this soil environment. When considering the decomposition of human remains specifically, these combined biogeochemical and ecological shifts have the potential to be harnessed as a forensic tool for refining time-since-death estimates, or the postmortem interval (PMI) (Metcalf et al. 2016, Adserias-Garriga et al. 2017, Singh et al. 2018, DeBruyn et al. 2021, Mason et al. 2022).

Assessments of biogeochemical changes within decomposition-impacted soils (both human and animal) have included a wide variety of parameters: pH (Keenan et al. 2018b, Quaggiotto et al. 2019, DeBruyn et al. 2021, Mason et al. 2022, Taylor et al. 2023), soil electrical conductivity (EC; Fancher et al. 2017, Keenan et al. 2018b, Quaggiotto et al. 2019, Mason et al. 2022, Taylor et al. 2023), organic and inorganic C and N compounds (Towne 2000, Aitkenhead-Peterson et al. 2012, Szelecz et al. 2018, Keenan et al. 2018b, DeBruyn et al. 2021), respiration (Cobaugh et al. 2015, Keenan et al. 2018b, Mason et al. 2022), soil oxygen (Keenan et al. 2018b), elemental analysis (Parmenter and MacMahon 2009, Aitkenhead-Peterson et al. 2012, Perrault and Forbes 2016, Fancher et al. 2017, Taylor et al. 2023), extracellular enzyme activity (Keenan et al. 2018a, b, DeBruyn et al. 2021, Mason et al. 2022), protein, fatty acid, steroid, and peptide concentrations (Macdonald et al. 2014, Lühe et al. 2017, 2018, Keenan et al. 2018b), naturally occurring stable isotope fractionation (Keenan et al. 2019), and metabolomics and lipidomics (DeBruyn et al. 2021). These diverse parameters have all demonstrated soil responses to decomposition on varied times scales from days to months, and to a limited extent across seasons (Meyer et al. 2013, Perrault and Forbes 2016, DeBruyn et al. 2021). Soil pH is typically altered, and direction of the pH response varies in part between species;

Received 9 March 2024; **revised** 8 July 2024; **accepted** 17 September 2024

soil acidification is often observed associated with humans and alkalinization with animals (but see: Szelecz et al. 2018, Keenan et al. 2018b, Quaggiotto et al. 2019, DeBruyn et al. 2021, Mason et al. 2022, Taylor et al. 2023). EC increases immediately upon decomposition fluids entering the soil. Fluctuations observed in C and N compounds, respiration rates, and enzyme activity show promise as indicators of early periods of decomposition (active through advanced decay) where most soft tissue mass is lost; C and N transformations are related to increased heterotrophic microbial activity and accompanying oxygen use within the soil (Keenan et al. 2018b). Terrestrial microbial ecology studies have shown that pH and EC (the latter often expressed in terms of salinity or ionic strength) are strong drivers of bacterial community structure across ecosystems (Rousk et al. 2010, Rath et al. 2019). Likewise, organisms responsible for soil nitrogen cycling have a demonstrated sensitivity to both pH and soil oxygenation (Dent et al. 2004). Therefore, it has been assumed that selective pressures exerted on soil microbial communities originating from decomposition-induced changes in soil pH, redox status, and EC result in profound alterations to microbial community structure and function over time.

In recent years, advances in sequencing technology have made it possible to create longitudinal surveys of decomposition-related microbial community successional patterns (Mason et al. 2023). There has been interest in whether these patterns could be used to estimate PMI, inspired by forensic entomology and predicated on the hypothesis that following the release of decomposition products into the soil, microbial decomposer communities in the soil exhibit consistently repeatable successional patterns over time as they respond to the nutrient influx. The majority of studies characterizing the soil postmortem microbiome (or "necrobiome") have focused on exploring bacterial community composition and successional patterns (Lauber et al. 2014, Carter et al. 2015, Cobaugh et al. 2015, Metcalf et al. 2016, Adserias-Garriga et al. 2017, Singh et al. 2018, Procopio et al. 2019, Burcham et al. 2021, Mason et al. 2022). By comparison, the exploration of changes within fungal communities has received less attention, but they also appear to exhibit some repeatable successional patterns (Metcalf et al. 2013, 2016, Carter et al. 2015, Weiss et al. 2016, Fu et al. 2019, Procopio et al. 2020, Mason et al. 2022). Soil fungi are key decomposers of organic material and tolerate much wider pH ranges than do bacteria (de Boer et al. 2005, Rousk et al. 2010) leading to the hypothesis that fungi may be important decomposers in the acidic soils frequently associated with human decompositon. While the focus of this collective body of work has centered on identifying changes to the postmortem microbiome structure and diversity, there are several notable omissions in these prior studies: (1) studies have been primarily focused on the early period of decomposition in which soft tissue mass loss is greatest and not later time periods; (2) studies have included only limited environmental, soil, or seasonal explanatory data to aid in interpretation of microbial community compositional changes; (3) there are few direct comparisons of warm versus cool season decomposition dynamics; and (4) microbiome studies generally do not quantify microbial abundances or biomass to link community compositional changes to determine potential functional impact. Furthermore, many forensics-focused studies use animals as a human proxy (e.g. pig), despite increasing evidence that decomposition patterns vary between species due to a variety of considerations that include size, tissue composition, and scavenger preference (Notter et al. 2009, Dautartas et al. 2018, Steadman et al. 2018, Barton et al. 2020, DeBruyn et al. 2021).

To address these knowledge gaps, we designed a pair of surface human decomposition studies with the following objectives: (1) characterize seasonal differences in biogeochemistry, microbial (bacterial and fungal) community composition, and microbial abundances with high temporal resolution over 1 year; and (2) integrate patterns observed in soil biogeochemistry with those of bacterial and fungal community structure to identify potential drivers of microbial succession. To control as many variables as possible, we (1) used replicate human donors of similar mass to control for interindividual variation in size; (2) placed donors simultaneously in the field so that environmental conditions within each seasonal trial would be the same; and (3) monitored local temperatures to allow for direct comparison between seasonal trials based on accumulated thermal units. We hypothesized that we would observe different seasonal patterns in both biogeochemistry and microbial community succession due to differences in external temperatures, variations in deposition rates of decomposition products (i.e. "pulse" events in warm weather as opposed to the slow release of materials in cooler weather) and the presence or absence of insect activity. We further hypothesized that these collective differences would vary by soil depth as decomposition products translocated to subsoils.

Materials and methods

Experimental site

This study took place at the University of Tennessee Anthropology Research Facility (ARF), Knoxville, TN, USA. The ARF is part of the University of Tennessee Forensic Anthropology Center (FAC) and is the longest running outdoor human decomposition facility in the USA, in service since 1981 (Damann et al. 2012). The site is composed of temperate mixed deciduous forest, with a Köppen climate classification of *Cfa* (humid subtropical). Soils belong to the Loyston–Talbott–Rock outcrop and Coghill–Corryton complexes (Hartgrove 2006, Soil Survey Staff 2018), and are composed of the following clay minerals: vermiculite, mica, interstratified mica–vermiculite, and kaolinite (Taylor et al. 2023).

Site layout and donor placement

A total of six deceased human subjects (hereafter, "donors") were used for this study, who were whole body donors to the FAC (https://fac.utk.edu/body-donation/) to be used specifically for the purpose of decomposition research. No living human subjects were involved, therefore this study was exempt from review by the University of Tennessee Institutional Review Board. No preferences were made for ancestry, sex, height, or age. Donors had not been autopsied nor had they sustained physical trauma that might potentially create artificial points of ingress for scavengers, insects, or microbes. Donors within a weight range of 68.5–91.6 kg were selected to reduce variability due to mass. Field placement sites were chosen within new sectors of the ARF that had not previously been used for surface or burial decomposition experiments. Spring and winter trials were located ~20 m apart (Supplementary file 1: Fig. S1).

Spring 2018: three male donors within a weight range of 90.7–91.6 kg (200–202 lbs) were accepted for this study. Heights ranged from 1.76 to 1.81 m, and body mass index (BMI) values ranged from 27.7 to 29.6 (Supplementary file 1: Table S1). Data were collected from 2 May 2018 through 13 May 2019 (376 days), and consisted of daily photographs, visual assessment of decomposition stages, and total body scores (TBS) according to Payne (1965) and Megyesi et al. (2005), local environmental data, and soil samples for soil chemistry and DNA extraction.

Winter 2019: three male donors within a weight range of 68.5–87.1 kg (151–192 lbs) were accepted for this study (Supplementary file 1: Table S1). These donors were placed 9 months after the start of the spring 2018 study in order to capture seasonal differences in decomposition patterns. Heights differed within 20 cm, and BMI values ranged from 24.7 to 29.4. Data collection began on 8 February 2019 and continued through 27 February 2020 (384 days).

For both trials, temperature probes (Decagon Devices, RT-1) were inserted internally (rectally) into each donor prior to placement, and donors were immediately frozen. The still-frozen donors were simultaneously placed at the study site unclothed, supine, and in direct contact with the soil surface to allow insect and scavenger access. Donors were spaced 2 m apart (Supplementary file 1: Fig. S1), which previous research has shown is sufficient space to prevent cross-contamination from decomposition products: in our previous study, lateral transport of decomposition products in soil has not been found appreciable beyond 50 cm, and vertical translocation below ~20 cm (Keenan et al. 2018a). Additional sensors (Decagon Devices, GS3) were placed in the soil underneath each donor to measure soil temperature, moisture, and EC. A third set of sensors were placed ~50 cm above the soil surface to record local ambient air temperature. Placement of these sensors was designed to avoid the influence of elevated cadaver temperatures during decomposition.

Sample collection

Soil samples were collected at 20 time points throughout the spring study, and at 19 points during the winter study. The first four samples in each seasonal study were selected based on visual assessments of decomposition stages: initial field placement, day 0; bloat, day 8 (spring) or day 21 (winter); active decay, day 12 (spring) or day 38 (winter); onset of advanced decay, day 16 (spring) or days 55–75 (winter). Once advanced decay had begun, sampling continued at approximately evenly spaced intervals based upon equivalent thermal units: 8400 accumulated degree hours (ADH) or 350 accumulated degree days (ADD), as calculated by local ambient air temperature measurements with a baseline threshold of 0°C. For the spring study, the remainder of the sampling dates corresponded to days 27, 43, 58, 72, 86, 103, 117, 132, 150, 168, 201, 254, 303, 340, 357, and 376, with skeletonization occurring by day 303. For the winter study, the remainder of the sampling dates corresponded to days 94, 110, 126, 140, 158, 172, 186, 201, 216, 234, 252, 290, 335, and 384, with skeletonization occurring by day 158 (Tables 1 and 2).

Soil sampling was performed using a 1.9-cm (three-fourth inch) diameter soil auger to remove five 16-cm cores (or sufficient soil to equal 200 g) from underneath each donor as well as from paired control plots located between 2 and 3 m upslope from each donor. Cores were divided into two depth segments: 0–1 and 1–16 cm, and soils from each depth were composited to create single samples from underneath each donor and from control plots. This 1-cm depth sample was referred to as an interface sample and was designed to capture hot-spot effects in the immediate proximity to decomposing remains. Dissolved oxygen (DO) was measured underneath donors and in controls using an Orion Star A329 multiparameter meter (ThermoScientific). A total of 12 samples were collected per sampling time point (six cores and six interfaces). Samples were transported back to the laboratory, where soil aliquots for DNA extraction were flash-frozen and stored at −80°C. All other soils were stored at 4°C and were processed within 48 h.

Soil physical and chemical analyses

Particle size analysis (PSA) was performed on homogenized control soils to verify similarity of field placement sites. Air-dried soils were sieved with 2-mm sieves, and organic matter was removed. PSA was performed using a Malvern Mastersizer 3000 laser particle size diffractor. Soil chemical analyses followed methods described in Keenan et al. (2018a, b). Briefly, soils were homogenized, and debris >2 mm (rocks and insects) were removed. Gravimetric moisture was calculated from mass loss following oven drying for 72 h at 105°C. Oven-dried soils were ground and analysed for total carbon (TC) and total nitrogen (TN) using a Vario Max CN Elemental Analyser (Elementar, Hanau, Germany). Soil pH and EC were measured on soil slurries of 1:2 soil:deionized water using an Orion Star A329 multiparameter meter (ThermoScientific). Respiration rates were assessed according to protocols outlined in Keenan et al. (2018a, b). Briefly, soils were sealed in 60 ml serum vials, and 0.5 ml headspace aliquots were removed immediately after sealing (T0), and again following a 24-h incubation (T24) at 20°C. Measurements were conducted in duplicate using a LI-820 CO_2 gas analyser and consisted of injection of 0.5 ml of the serum vial headspace. Soils were extracted in 0.5 M K_2SO_4, 1:4 parts soil and salt solution. Slurries were shaken at room temperature for 4 h at 160 r m^{-1}, after which they were allowed to settle and then vacuum-filtered using 1 µm glass microfiber filters (Ahlstrom). Filtrates were stored at −20°C until downstream processing. Ammonium and nitrate in filtrates were quantified colorimetrically in triplicate according to protocols described in Keenan et al. (2018a, b).

DNA extraction, library preparation, sequence processing, and quantitative PCR

Prior to DNA extraction, replicate control samples for interfaces (0–1 cm) and cores (1–16 cm) were each pooled into single samples by equal weight per sample. Impacted soils were not pooled. This yielded eight extractions per sampling time point: three impacted interfaces, three impacted cores, one pooled control interface, and one pooled control core. The DNA was extracted from 250 mg soil samples using the QIAGEN DNeasy® PowerLyzer® PowerSoil® Kit (Hilden, Germany) according to manufacturer's protocols, and included a prolonged bead beating step (4000 r m^{-1} for 45 s) recommended for soils with high clay content. Concentrations were quantified using a NanoDrop One spectrophotometer (ThermoScientific). Library preparation and sequencing was performed on the Illumina MiSeq platform at the Genomics Core Facility at the University of Tennessee, Knoxville. Sample preparation for amplicon sequencing consisted of polymerase chain reaction (PCR) amplification of the bacterial 16S rRNA region using universal primers 515F and 806R (Apprill et al. 2015, Parada et al. 2016). Preparation for amplicon sequencing of the fungal ITS2 rRNA region used a mixture of primers (six forward and two reverse: ITS3NGS1, ITS3NGS2, ITS3NGS3, ITS3NGS4, ITS3NGS5, ITS3NGS10, ITS4NGR, and ARCH-ITS4) as previously described (Cregger et al. 2018), to amplify regions of ~300–400 nucleotides in length. Samples were diluted 1:10 for amplification and PCR amplification was performed using 12.5 µl 2x KAPA HiFi HotStart ReadyMix Taq (Roche, Indianapolis, IN), 5 µL each of 1.5 µM forward and reverse primers, and 2.5 µl sample, for a total volume of 25 µl per sample. The PCR amplification protocol consisted of denaturation at 95°C for 3 min followed by 30 cycles of denaturation (95°C for 30 s), annealing (55°C for 30 s), and extension at (72°C for 30 s), and a final elongation for 5 min at 72°C. Results were visualized by gel electrophoresis. Cleanup of PCR products was

Table 1. Spring 2018 donor sampling.

Study day	Study date (D-M-Y)	ADH ambient	ADD	ADH internal	ADH donor soil	ADH soil control	Morphological decomposition stage
0	2 May 2018	0	0	0	0	0	Initial
8	10 May 2018	3801	164	2457	2703	3525	Bloat
12	14 May 2018	6036	257	5352	5362	5578	Active decay
16	18 May 2018	8180	346	8528	8360	7648	Advanced 1
27	29 May 2018	14 213	598	17 814	18 289	13 501	Advanced 2
43	14 June 2018	23 070	967	29 967	30 771	22 104	Advanced 3
58	29 June 2018	31 864	1334	40 296	41 581	30 707	Advanced 4
72	13 July 2018	40 428	1691	50 757	51 922	38 979	Advanced 5
86	27 July 2018	48 562	2030	60 190	61 203	46 965	Advanced 6
103	13 August 2018	58 224	2432	70 875	71 557	56 530	Advanced 7
117	27 August 2018	66 125	2761	79 316	79 553	64 310	Advanced 8
132	11 September 2018	75 002	3131	88 381	88 547	73 013	Advanced 9
150	29 September 2018	85 018	3548	98 590	98 759	82 971	Advanced 10
168	17 October 2018	93 873	3917	107 592	107 850	91 879	Advanced 11
201	19 November 2018	101 688	4242	115 703	116 954	100 777	Advanced 12
254	11 January 2019	110 453	4608	124 074	127 477	110 492	Advanced 13
303	1 March 2019	118 303	4935	131 337	135 944	118 509	Skeletonization 1
340	7 April 2019	127 298	5310	140 332	144 538	127 166	Skeletonization 2
357	24 April 2019	134 033	5590	147 067	151 096	133 676	Skeletonization 3
376	13 May 2019	143 017	5964	156 051	159 517	142 144	Skeletonization 4

Date of sampling, associated study day, ADH calculated from hourly ambient air, internal donor, and soil temperature data are shown, along with morphological decomposition stage. ADD are calculated from daily mean temperatures. Decomposition stages that include more than one sampling time point are numbered sequentially. Beginning in advanced decay, sampling occurred at ~8400 ADH intervals based off ambient air temperatures.

Table 2. Winter 2019 donor sampling.

Study day	Study date (D-M-Y)	ADH ambient	ADD	ADH internal	ADH donor soil	ADH soil control	Morphological decomposition stage
0	8 February 2019	0	0	0	0	0	Initial
21	1 March 2019	3992	167	3319	3826	4010	Bloat
38	18 March 2019	7485	312	6968	7594	7453	Active decay
55	4 April 2019	11 788	492	11 662	12 127	11 595	Active/Advanced
75	24 April 2019	19 721	822	20 608	22 782	18 981	Advanced 1
94	13 May 2019	28 705	1196	30 224	33 575	27 346	Advanced 2
110	29 May 2019	37 257	1553	39 027	43 005	35 304	Advanced 3
126	14 June 2019	45 760	1907	48 411	52 404	43 466	Advanced 4
140	28 June 2019	53 497	2229	56 443	60 714	50 813	Advanced 5
158	16 July 2019	64 369	2682	67 393	71 952	61 169	Skeletonization 1
172	30 July 2019	72 486	3021	75 351	79 891	68 939	Skeletonization 2
186	13 August 2019	80 717	3364	83 391	87 883	76 821	Skeletonization 3
201	28 August 2019	89 634	3735	92 077	96 552	85 440	Skeletonization 4
216	12 September 2019	98 415	4101	100 397	104 845	93 794	Skeletonization 5
234	30 September 2019	109 169	4549	110 723	115 079	104 141	Skeletonization 6
252	18 October 2019	117 661	4903	119 031	123 576	112 587	Skeletonization 7
290	25 November 2019	126 681	5279	128 883	134 019	122 428	Skeletonization 8
335	9 January 2020	134 896	5621	136 943	142 473	130 809	Skeletonization 9
384	27 February 2020	143 611	5984	144 936	151 104	139 403	Skeletonization 10

Date of sampling, associated study day, ADH calculated from hourly ambient air, internal donor, and soil temperature data are shown, along with morphological decomposition stage. ADD are calculated from daily mean temperatures. Decomposition stages that include more than one sampling time point are numbered sequentially. Beginning in advanced decay, sampling occurred at ~8400 ADH intervals based off ambient air temperatures.

performed using AMPure beads (Agencourt, Beverly, MA). A second indexing PCR was performed using Nextera XT indexes with PCR cycling performed as described above except with eight cycles of elongation. Index PCR cleanup was again performed using AMPure beads, and final quality and concentrations were determined on a Bioanalyzer (Agilent, Santa Clara, CA). Samples were pooled to a final loading concentration of 4 pM, combined with 15% PhiX, and paired-end sequencing performed on a v3 flow cell on the Illumina MiSeq sequencing platform. Raw sequence reads are deposited in the NCBI Short Read Archive under BioProjects PRJNA1066312 (Spring data set) and PRJNA1070662 (Winter data set).

Quality control of bacterial 16S sequence reads was performed using MOTHUR (v. 1.44.0) (Schloss et al. 2009). Briefly, paired end reads were merged and primers were trimmed, allowing a maximum of two nucleotide differences on both forward and reverse primers. Sequences were screened to remove ambiguous bases, sequences shorter than 50 bp, and longer than 275 bp. Sequences were aligned to the SILVA v132 reference database (Quast et al. 2013), overhangs were removed, and sequences with two

or fewer differences were merged. Chimeras were removed using VSEARCH, sequences were classified, and unwanted lineages (chloroplast, mitochondria, unknown, archaea, and Eukaryota) were removed. Sequences were clustered into operational taxonomic units (OTUs) at 97% similarity.

Quality control of fungal ITS reads was performed using a customized MOTHUR (v. 1.44.0) pipeline (Schloss et al. 2009). Paired end reads were merged, and primers were trimmed, as described for 16S sequences. Reads were screened to remove sequences with ambiguous bases and read lengths shorter than 200 bp. Initial clustering was performed, allowing up to three nucleotide differences between sequences. Chimeras were removed using VSEARCH, and remaining sequences were mapped to the UNITE 8.2 reference database using the standard cutoff of 80% (Abarenkov et al. 2020). Unwanted lineages were removed (unknown, Protista, protozoa, Plantae, Chromista, bacteria, and Animalia). Since ITS sequences are of differing length, sequences were clustered into OTUs using greedy clustering with a cutoff of 0.05 in VSEARCH.

The PCR blanks and test data were removed from all datasets, and alpha diversity indices (Shannon, Inverse Simpson, and Chao1 were calculated in R using Phyloseq; Bioconductor BiocManager 1.30.10) (McMurdie and Holmes 2013) following both the removal of singletons and doubletons. Removal of singletons resulted in 8098 ITS OTUs and 19 591 16S OTUs for the spring dataset, and 7846 ITS OTUs and 16 388 16S OTUs for the winter dataset. Removal of doubletons resulted in 6021 ITS OTUs and 15 861 16S OTUs from the spring dataset and 5808 ITS OTUs and 13 089 16S OTUs from the winter dataset. For both seasons changes to diversity were negligible between removal of singletons and doubletons; since our focus was to determine robust patterns of change rather than identifying changes to rare taxa, we have selected removal of doubletons for all downstream analyses.

Bacterial and fungal quantities were estimated using quantitative PCR (qPCR) of rRNA genes as a proxy. The Femto™ Fungal DNA Quantification Kit and Femto™ Bacterial DNA Quantification Kit (Zymo Research Corporation, Irvine, CA) were used according to manufacturer protocols. The qPCR was performed on a Bio-Rad CFX Connect Real-Time PCR Detection System (Bio-Rad Laboratories, Inc., Hercules, CA). Three outliers showing poor or no amplification were removed from the dataset.

Statistical analyses

Donors ($n = 3$ in the spring, and $n = 3$ in the winter) were treated as experimental replicates, each with a paired control site. Shapiro–Wilk tests were performed, which showed that data was not normally distributed over the course of the study, so nonparametric Kruskal–Wallace ($P < .05$) was used to test for differences between treatments (impacted soils underneath donors and controls). Student's *t*-tests were conducted at each sampling time point to determine if impacted soils significantly differed from controls. Canonical analysis of principal coordinates (CAP) on Bray–Curtis distances of community compositional data was performed followed by PERMANOVA ($P < .05$) in order to test for relationships between biogeochemical variables and changes in microbial beta diversity by study day. DO values for interfaces were extrapolated from core data, and data following day 168 (spring trial) and 201 (winter trial) were estimated to remain at 100%. Analyses and visualizations were conducted in R (version 3.6.1) using the tidyverse (1.2.1), vegan (version 2.5–6), ggplot2 (version 3.2.1), RColorBrewer (version 1.1–2), and Phyloseq (Bioconductor BiocManager 1.30.10) packages (R Development Core Team 2010, McMurdie and Holmes 2013, Neuwirth 2014, Berry 2016, Wickham 2016, 2017, Oksanen et al. 2019). Analysis files and R code are available at: https://github.com/jdebruyn/ARF-seasonal.

Results

Decomposition stages

Spring 2018: three frozen donors were placed at the study site on 2 May 2018 (day 0) (Supplementary file 1: Fig. S1). Fly egg masses were visible in the nasal cavities of all donors within 24 h, and by day 2 extensive fly egg oviposition was evident throughout facial areas (Supplementary file 1: Table S2). Internal temperatures of the donors equilibrated with ambient air temperatures by day 4 when the first evidence of bloating was visible on the lateral abdomens (Table S2, Fig. S2). Donors exhibited extensive bloating by day 8. Bloating decreased by day 12 and there was visible fluid release into the soil, marking the beginning of active decay. Larval masses visibly peaked between days 13 and 15. By day 16 visible cadaver decomposition islands (CDIs) were well-developed, substantial tissue loss was evident, and visible changes in decomposition progression had slowed, marking the beginning of advanced decay. During the latter period of advanced decay (day 86 onwards) interindividual variation of tissue loss was apparent. Generally, soils beneath donors were initially greasy, followed by the development of hard soil crusts. Intermittent white fungal growth and the development of pockets of adipocere were also observed. Skeletonization or partial mummification began following day 303.

Winter 2019: a second set of three frozen donors was placed at the ARF nearby the first trio of donors on 8 February 2019, such that local environmental and edaphic conditions as well as forest canopy and understory conditions were similar (Supplementary file 1: Fig. S1). By day 7, internal donor temperatures had equilibrated with ambient temperatures (Supplementary file 1: Table S3, Fig. S3). Donors were sampled on day 21, around the onset of bloat (Supplementary file 1: Table S3, Fig. S3). The bloat stage was less-well defined than in the spring study and consisted of only slight bloating with a continuous seepage of decomposition fluid. No signs of insect activity were observed during any of the early stages of decay. Minor scavenging was observed during early decay and limited to extremities. Active decay was estimated to begin on day 38; CDIs became well-developed, and adipocere was observed in soils under the torsos. Since soft tissue mass loss was gradual, samples were collected on both days 55 and 75, representing "active-advanced" and "advanced decay 1," respectively. During the latter period of advanced decay adipocere quantities reduced and fungal growth was observed on soils underneath donors. Gradual mass loss continued with very little interindividual variation in decomposition rates observed between the three donors. Donors were mostly skeletonized or mummified by day 158.

Comprehensive field notes, including TBS (based on visual scoring) can be found in the supplementary materials (Supplementary file 1: Tables S2 and S3, Fig. S4).

Environmental sensor data

Spring 2018: following donor internal and ambient temperature equilibration, both internal and impacted soil temperatures increased above ambient air temperatures by day 8, the point at which donors were fully bloated (Supplementary file 1: Fig. S2A). Elevated temperatures continued through day 80, and ranged from 41.3°C to 45.6°C, commensurate with the greatest visible

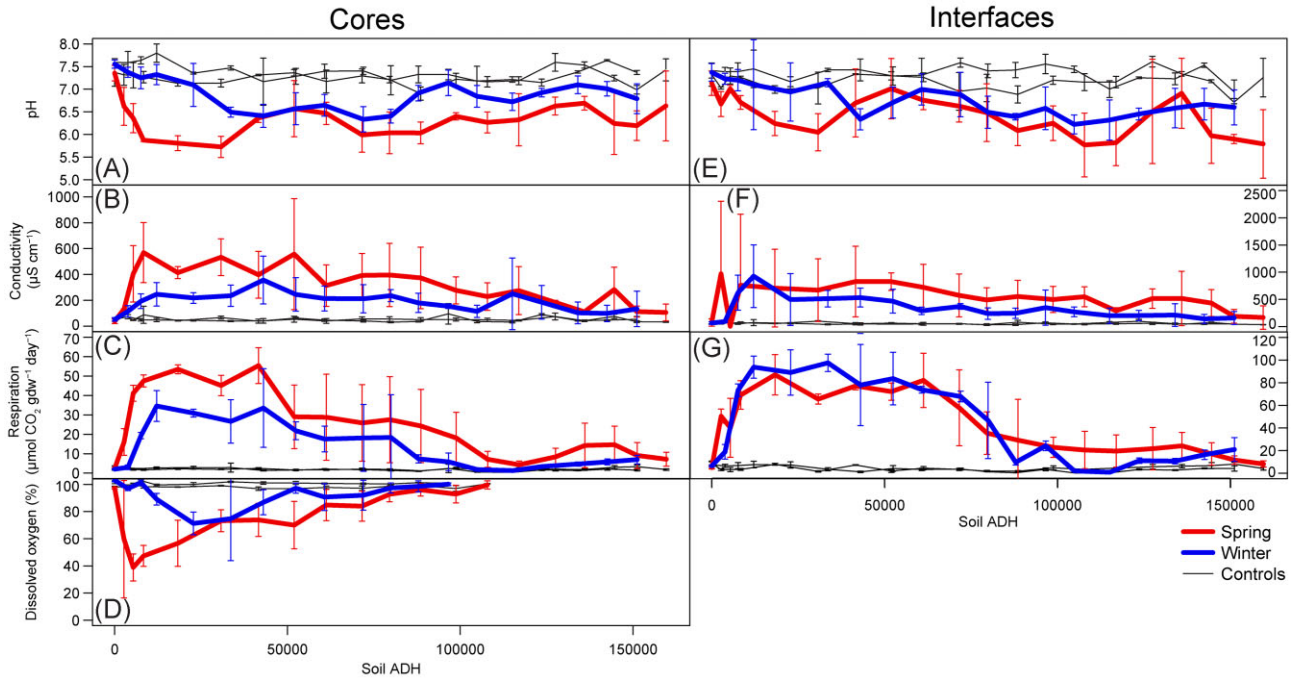

Figure 1. Seasonal comparisons between biogeochemical variables in core and interface soils. The magnitude and timing of changes in (A and E) pH, (B and F) conductivity, (C and G) CO_2, and (D) DO in core (1–16 cm) and interface (0–1 cm) soils are presented in units of equivalent thermal units based upon soil temperatures (soil ADH). Means and standard deviations are shown ($n = 3$).

larval masses. Maximum soil temperatures underneath donors reached 40.2°C–42.8°C corresponding to days 23–24. Ambient air and soil control temperatures did not differ from one another. Soil moisture increased immediately upon donor placement and remained elevated for the majority of the study. The largest increase above control values occurred between days 91 and 122 in the latter half of advanced decay, when soils were still covered by donor remains as well as a hard crust of decomposition materials (Supplementary file 1: Fig. S2B). Soil moisture maxima in decomposition soils ranged from 52.1% to 54.7% volumetric water content (%VWC). EC data originating from soil sensors was similar to that measured in core and interface in the lab; sensor prongs extended ~6 cm into the soil, thus homogenized patterns reported for respective sampling depths. Graphical data is presented here for reference (Supplementary file 1: Fig. S2C).

Winter 2019: in contrast to patterns observed in the spring, there was no difference between internal, ambient, and soil temperatures in the winter study, nor were differences observed between impacted soils and controls for moisture. Conductivity increased immediately after donor placement, remaining elevated through day 210 (Supplementary file 1: Figs S3 and S5).

For both seasonal datasets, cumulative increases in temperatures reflect similarities between ambient air and soil control temperatures, as well as similarities between donor and impacted soil temperatures, as noted above; patterns in cumulative temperature differ, as do final cumulative temperatures at the end of the study (Tables 1 and 2).

Soil biogeochemistry

Soils for the spring donor site were composed of 6.34% sand, 85.02% silt, and 8.64% clay. Soils from the winter site were composed of 10.96% sand, 81.44% silt, and 7.6% clay.

Spring 2018 core (1–16 cm) samples. Over the course of the entire study, all measured soil chemical parameters in decomposition-impacted cores differed from controls with the exceptions of TN and the C:N ratio (Kruskal–Wallace, $P < .05$) (Supplementary file 1: Table S4). The first changes to soil chemistry were detected during the bloat phase (day 8; 2703 ADH based on donor soil), when the first evidence of fluid seepage into the soil was visible (Figs 1 and 2, Table 3; Supplementary file 1: Table S5). Following this bloat period, soil acidified and remained acidic for the majority of the study. Decomposition products stimulated heterotrophic respiration, resulting in reductions in soil oxygen and nitrate during active decay (day 12; 5362 ADH); mean DO decreased to 38.9% and nitrate concentrations decreased below background levels falling to below 50% of control concentrations. Respiration rates continued to increase, reaching a maximum of 55.4 ± 9.20 µmol CO_2 per gram dry weight per day (gdw^{-1} day^{-1}) on day 58. Both TC and the C:N ratio in decomposition soils were significantly elevated on day 27 (18 289 ADH) during early advanced decay, at 11.7 ± 2.3%C and 16.8 ± 0.5, respectively. TN in impacted soils ranged from 0.39 to 0.77% N but did not vary significantly from control soils (0.37 to 0.6% N). Ammonium concentrations in decomposition soils increased in conjunction with increases in EC, becoming significantly different from control soils by day 8 (2703 ADH) and exhibiting maximum concentrations during early advanced decay (day 16; 8360 ADH) at 665.2 ± 375.6 µg gdw^{-1} and 568.7 ± 232.3 µS cm^{-1}, respectively. Following soil oxygen recovery on day 168 (107 850 ADH), nitrification began to occur and nitrate concentrations steadily increased to a maximum during skeletonization (day 340; 144 538 ADH) at 101.2 ± 85.2 µg gdw^{-1}. By the end of the study no parameters exhibited significant differences between decomposition soils and controls, however mean values and wide standard deviations indicate that some degree of impaction was still evident.

Spring 2018 interface (0–1 cm) samples. All measured parameters in impacted interface soils were altered during decomposition compared to controls (Kruskal–Wallace, $P < .05$) (Supplementary file 1: Table S4). Overall response patterns were

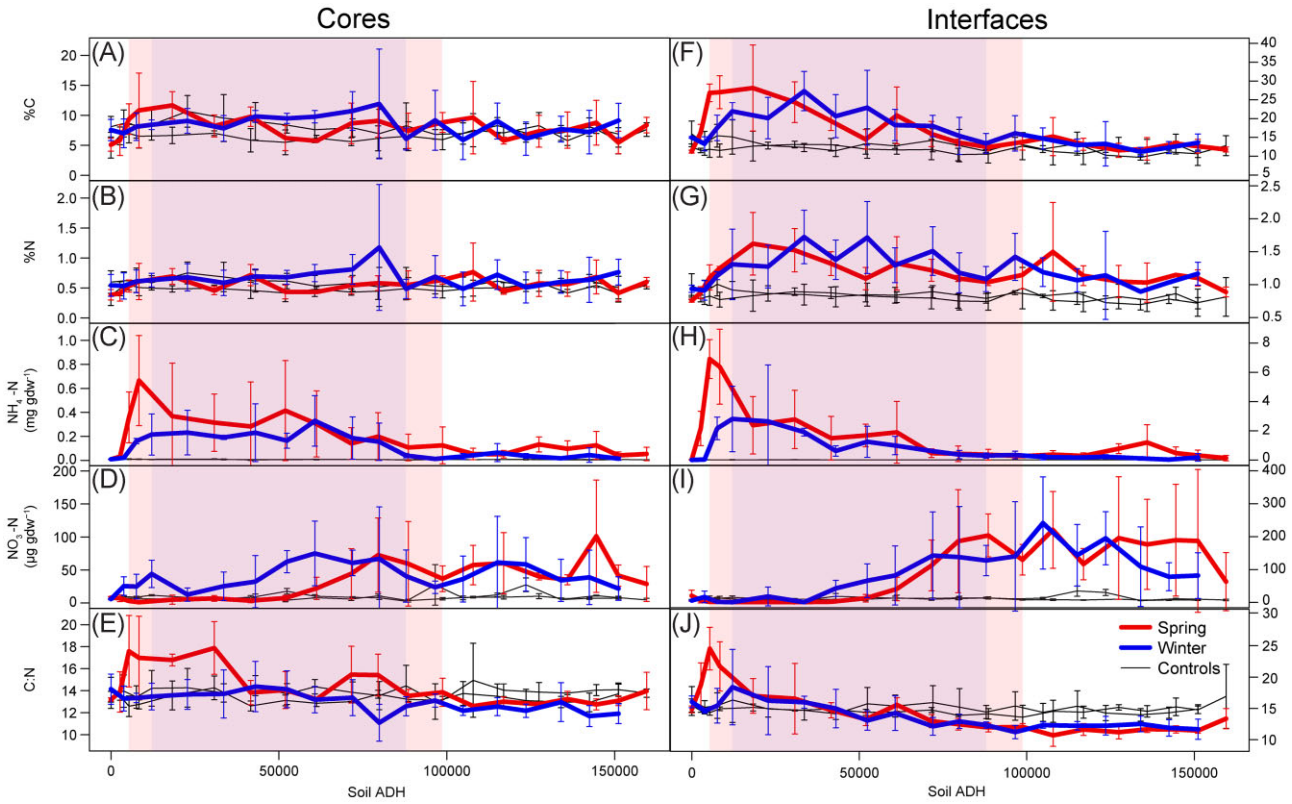

Figure 2. Seasonal comparisons between carbon and nitrogen in core and interface soils. The magnitude and timing of changes in soil (A and F) TC (expressed as %C), (B and G) TN (%N), (C and H) NH_4-N, (D and I) NO_3-N, and (E and J) the carbon: nitrogen ratio in core (1–16 cm) and interface (0–1 cm) soils are presented in units of equivalent thermal units based upon soil temperatures (soil ADH). Means and standard deviations are shown (n = 3). Shaded areas correspond to the periods of reduced soil oxygen for the spring (lighter shading) and winter (darker shading).

consistent with those observed in core soils, however there was greater variability in the interfaces; i.e. changes were greater in magnitude in decomposition soils both in terms of mean values and standard deviations, frequently leading to statistical non-significance (Figs 1 and 2, Table 4; Supplementary file 1: Table S5). An especially noteworthy example of this occurred in ammonium; initial significant increases coincided with the maximum soil concentration on day 12 (6905.5 ± 1325.3 µg gdw^{-1} a 500x increase over controls), however the following sampling time period had a similar mean, but doubled variance. Mean EC reached a maximum of 969.1 ± 1336.7 µS cm^{-1} during bloat immediately followed by a brief decrease to 4.0 ± 0.9 µS cm^{-1} during active decay; this decrease occurred during the initial presence of "greasy" decomposition products in soil samples and extracts and was observed in soils associated with all three donors. Shifts in inorganic N pools (ammonium and nitrate) reflected core patterns, except at higher soil concentrations, and early nitrate decreases below control values were apparent throughout the period in which soil oxygen was <75%. TC and TN were both significantly elevated by day 16, and reached maxima on day 27, both at approximately twice core values. Over the course of the study TC returned to control values in mid-advanced decay, however TN remained elevated throughout, in part due to the respective timing and soil concentrations of ammonium and nitrate. The C:N ratio reflected both patterns in TC and TN: brief elevation on day 12 corresponding to increased TC abundances, followed by an extended period (days 132–357) in which the C:N ratio fell below that of control soils corresponding to the period in which TC recovered to control values but TN remained elevated.

Winter 2019 core (1–16 cm) samples. Soil chemical parameters in decomposition-impacted core soils significantly differed from control soils with the exceptions of TN and TC (Kruskal–Wallace, $P < .05$) (Supplementary file 1: Table S6). In comparison with immediate soil responses apparent during bloat and active decay in the spring study, parameters in the winter study underwent more gradual change with maxima or minima occurring in advanced decay and skeletonization (Figs 1 and 2, Table 5; Supplementary file 1: Table S7). Mean soil pH gradually became acidic, reaching only 6.3 ± 0.3 in early skeletonization (day 158; 71 952 ADH) in contrast with spring cores which reached 5.7 ± 0.2 by early advanced decay. Respiration rates reached maximum values in early advanced decay (day 55, 12 127 ADH) at concentrations only 62% of spring core samples. Likewise, soil oxygen levels declined gradually over 75 days, dropping to 71.3% of initial values, approximately half of the decrease observed in the spring trial. Ammonium increases were gradual and did not display the sharp increases observed in the spring trial; both ammonium and nitrate maxima occurred on day 140 (60 714 ADH) at 329.4 ± 210.5 and 75.7 ± 48.9 µg gdw^{-1}, respectively. Unlike patterns observed in spring core data, nitrate did not fall below control concentrations during (lesser) soil oxygen reductions. Instead, there was greater overlap of ammonium and nitrate concentrations in winter core data in comparison with the oxygen-dependent separation that was visible in the spring core data. Conductivity reached maximum values on day 110 (43 005 ADH) at 356.4 ± 184.9 µS cm^{-1}. TC and TN reached maxima on day 172 at 12.0 ± 9.1%C and 1.18 ± 1.05% N, respectively, both approximately double that of control soil values, but in a

Table 3. Spring 2018 soil chemical parameters in core soils (1–16 cm).

Study day	Location	pH	EC ($\mu S\ cm^{-1}$)	DO (%)	Respiration ($\mu mol\ CO_2\ gdw^{-1}\ day^{-1}$)	Ammonium ($\mu g\ gdw^{-1}$)	Nitrate ($\mu g\ gdw^{-1}$)	%N	%C	C:N
0	Donor	7.4 ± 0.2	39.7 ± 19.6	97.3 ± 0.7	2.4 ± 0.4	8.9 ± 1.8	8.1 ± 1.8	0.39 ± 0.09	5.1 ± 1.1	13.2 ± 0.2
	Control	7.4 ± 0.3	31.3 ± 11.9	97.8 ± 0.9	2.9 ± 0.9	9.0 ± 2.3	7.3 ± 1.4	0.37 ± 0.16	5.0 ± 2.1	13.4 ± 0.5
8	Donor	6.6 ± 0.4	**131.7 ± 3.7****	59.7 ± 43.2	16 ± 6.9	**31.2 ± 5.8***	7.2 ± 5.1	0.41 ± 0.13	5.9 ± 2.6	13.9 ± 1.8
	Control	7.3 ± 0.2	81.4 ± 6.8	98.6 ± 0.8	2.8 ± 0.8	8.6 ± 1.2	6.3 ± 1.3	0.49 ± 0.12	6.6 ± 1.5	13.5 ± 0.4
12	Donor	**6.4 ± 0.3***	404.4 ± 217.7	**38.9 ± 10****	**41.2 ± 4.1****	357.4 ± 212.0	**3.1 ± 1.7***	0.53 ± 0.1	9.4 ± 2.6	17.6 ± 3.3
	Control	7.3 ± 0.3	48 ± 3.9	100.1 ± 0.9	2 ± 0.4	10.0 ± 2.7	7.8 ± 0.7	0.55 ± 0.08	7.0 ± 1.6	12.6 ± 0.9
16	Donor	**5.9 ± 0.0****	568.7 ± 232.3	**47.3 ± 7.7****	**47.5 ± 3.1****	665.2 ± 375.6	1.1 ± 0.7	0.61 ± 0.3	10.8 ± 6.2	17.0 ± 3.8
	Control	7.3 ± 0.1	87.9 ± 65.9	98.3 ± 1	1.7 ± 0.2	9.0 ± 1.9	6.1 ± 2.3	0.51 ± 0.14	6.5 ± 2.0	12.8 ± 0.4
27	Donor	**5.8 ± 0.2****	**413.8 ± 46.5****	56.6 ± 17	**53.5 ± 2.3*****	368.0 ± 443.1	5.0 ± 6.8	0.69 ± 0.13	**11.7 ± 2.3***	**16.8 ± 0.5***
	Control	7.1 ± 0.1	42.4 ± 2.3	98.1 ± 0.3	2.2 ± 0.3	9.8 ± 1.0	6.2 ± 1.0	0.49 ± 0.05	6.6 ± 1.4	13.6 ± 1.3
43	Donor	**5.7 ± 0.2****	**533.1 ± 142***	**73.3 ± 8***	**45.1 ± 5.2****	314.7 ± 239.2	6.9 ± 4.4	0.46 ± 0.07	8.2 ± 1.9	17.9 ± 2.4
	Control	7.1 ± 0.1	66.8 ± 11.7	99.1 ± 0.3	1.9 ± 0.2	10.4 ± 2.3	6.67 ± 2.5	0.49 ± 0.06	7.0 ± 0.4	14.3 ± 1.1
58	Donor	**6.4 ± 0.1****	397.4 ± 181.1	73.9 ± 12.2	**55.4 ± 9.2****	282.9 ± 371.1	3.5 ± 3.1	0.72 ± 0.18	9.8 ± 1.6	13.8 ± 1.1
	Control	7.3 ± 0.0	38.8 ± 14.9	96.8 ± 1.3	2.4 ± 0.4	3.8 ± 3.9	8.3 ± 2.9	0.46 ± 0.14	5.8 ± 1.9	12.6 ± 0.5
72	Donor	6.6 ± 0.6	557.3 ± 429	70 ± 17.4	29 ± 16.4	414.6 ± 417.2	7.5 ± 4.2	0.43 ± 0.11	6.2 ± 2.1	14.1 ± 1.7
	Control	7.4 ± 0.1	53.8 ± 22.6	96.8 ± 0.8	1.6 ± 0.1	5.7 ± 1.1	4.1 ± 2.2	0.42 ± 0.15	5.5 ± 2.1	13.1 ± 0.5
86	Donor	**6.5 ± 0.3***	314.2 ± 160.5	84.8 ± 11.5	28.8 ± 22.2	304.1 ± 275.7	22.2 ± 16.9	0.43 ± 0.02	5.7 ± 0.2	13.2 ± 0.2
	Control	7.2 ± 0.3	40.4 ± 17.9	97.8 ± 1.1	1.8 ± 0.4	6.8 ± 3.1	7.9 ± 2.9	0.48 ± 0.04	6.2 ± 0.5	12.9 ± 0.3
103	Donor	**6.0 ± 0.4***	392.7 ± 169.2	84 ± 11.1	25.9 ± 19.7	140.7 ± 132.2	44.4 ± 38.0	0.54 ± 0.14	8.7 ± 3.4	15.5 ± 2.6
	Control	7.3 ± 0.2	56.7 ± 15.8	97.2 ± 1.7	2 ± 0.5	6.7 ± 1.1	5.9 ± 2.3	0.43 ± 0.05	5.6 ± 0.7	13.0 ± 0.0
117	Donor	**6.0 ± 0.5***	395.9 ± 244.5	92.8 ± 5.6	27.5 ± 22.2	198.6 ± 199.4	72.6 ± 56.2	0.58 ± 0.12	9.1 ± 2.7	15.4 ± 1.9
	Control	7.2 ± 0.1	55.5 ± 18	98.6 ± 0.4	1.9 ± 0.3	7.4 ± 1.0	10.8 ± 2.9	0.45 ± 0.14	6.2 ± 2.1	13.7 ± 0.4
132	Donor	**6.0 ± 0.2****	373.6 ± 237.8	96 ± 4.6	24.3 ± 18.9	107.5 ± 110.9	59.4 ± 64.1	0.55 ± 0.24	7.4 ± 2.9	13.5 ± 0.6
	Control	6.9 ± 0.2	51.2 ± 14.8	99 ± 0.6	1.2 ± 0	2.6 ± 0.7	3.61 ± 2.2	0.49 ± 0.18	6.5 ± 2.4	13.2 ± 0.2
150	Donor	**6.4 ± 0.1****	277.3 ± 104.5	92.9 ± 6.5	18.1 ± 13.2	124.9 ± 153.7	36.7 ± 19.6	0.63 ± 0.07	8.8 ± 1.7	13.9 ± 1.3
	Control	7.2 ± 0.1	51.4 ± 12	97 ± 2.1	2.5 ± 0.5	7.6 ± 0.8	6.5 ± 1.8	0.45 ± 0.12	5.9 ± 1.7	13.1 ± 0.4
168	Donor	**6.3 ± 0.2****	229.1 ± 107	99.6 ± 3.1	7.1 ± 4.1	52.8 ± 47.7	57.5 ± 29.9	0.77 ± 0.48	9.6 ± 6.0	12.6 ± 0.2
	Control	7.2 ± 0.1	48.8 ± 13.1	100.5 ± 0.2	1.6 ± 0.1	6.0 ± 0.6	8.9 ± 1.2	0.5 ± 0.13	7.5 ± 2.8	14.9 ± 3.4
201	Donor	6.3 ± 0.6	275.2 ± 184.9		4.3 ± 2	50.5 ± 31.4	60.3 ± 46.4	0.45 ± 0.05	5.8 ± 0.6	13.0 ± 0.4
	Control	7.2 ± 0.1	44.6 ± 5.7		2.3 ± 0.5	8.1 ± 0.8	8.8 ± 2.7	0.5 ± 0.09	7.1 ± 1.3	14.0 ± 0.6
254	Donor	**6.6 ± 0.2****	**183.7 ± 16.5****		8.4 ± 4.5	132.7 ± 62.1	**40.2 ± 5.4****	0.58 ± 0.22	7.3 ± 2.7	12.8 ± 0.2
	Control	7.6 ± 0.2	74.4 ± 26.5		2 ± 0.9	8.5 ± 3.1	10.3 ± 3.8	0.6 ± 0.15	8.3 ± 2.2	13.9 ± 0.9
303	Donor	**6.7 ± 0.2****	**111 ± 15.1****		14.2 ± 11.5	96.8 ± 66.3	**35.2 ± 7.6***	0.56 ± 0.2	7.5 ± 3.0	13.2 ± 0.7
	Control	7.5 ± 0.1	42.2 ± 6.7		1.9 ± 0.4	7.1 ± 1.4	6.3 ± 0.5	0.42 ± 0.06	5.8 ± 0.8	13.8 ± 0.2
340	Donor	6.2 ± 0.7	282.8 ± 173.1		14.6 ± 9.5	125.2 ± 116.2	101.2 ± 85.2	0.68 ± 0.28	8.8 ± 3.7	**12.8 ± 0.5***
	Control	7.3 ± 0.1	75.6 ± 16.8		3 ± 0.8	8.5 ± 1.9	11.1 ± 0.7	0.54 ± 0.04	7.7 ± 0.7	14.1 ± 0.5
357	Donor	**6.2 ± 0.3***	112.8 ± 42.5		9.1 ± 6.7	41.3 ± 29.5	41.5 ± 16.2	0.42 ± 0.14	5.5 ± 1.9	13.1 ± 0.5
	Control	7.0 ± 0.1	34.7 ± 7.6		3.3 ± 0.8	7.7 ± 3.3	8.1 ± 2.2	0.41 ± 0.14	5.8 ± 2.2	14.1 ± 0.6
376	Donor	6.6 ± 0.8	106.2 ± 64.9		7.2 ± 3.6	53.1 ± 55.7	28.8 ± 26.4	0.6 ± 0.08	8.4 ± 1.3	14.0 ± 1.7
	Control	7.4 ± 0.2	33.1 ± 3.7		1.8 ± 0.4	4.2 ± 1.2	4.7 ± 2.3	0.55 ± 0.07	7.6 ± 1.1	13.8 ± 0.4

Data for pH, EC, DO, respiration, ammonium, nitrate, total N (%N), total C (%C), and the C:N ratio are shown for decomposition (donor) and control soils. Respiration, ammonium, and nitrate data are represented as per gram dry weight of soils (gdw). Data are means ± standard deviations for $n = 3$ replicate donors. Impacted soils that significantly differ from controls based upon Welch *t*-tests ($P < .05$) are presented in bold type. Data are means ± standard deviations for $n = 3$ replicate donors. Asterisks indicate levels of significance: *$P < .05$, **$P < .01$, and ***$P < .001$.

Table 4. Spring 2018 soil chemical parameters in interface soils (0–1 cm).

Study day	Location	pH	EC ($\mu S\ cm^{-1}$)	Respiration ($\mu mol\ CO_2\ gdw^{-1}\ day^{-1}$)	Ammonium ($\mu g\ gdw^{-1}$)	Nitrate ($\mu g\ gdw^{-1}$)	%N	%C	C:N
0	Donor	7.1 ± 0.3	73.7 ± 68.9	**5.1 ± 1.2***	22.8 ± 17.3	20.4 ± 16.8	0.76 ± 0.02	11.2 ± 0.4	14.9 ± 0.6
	Control	7.3 ± 0.3	43.8 ± 3.8	8.7 ± 1.5	19.4 ± 3.37	8.3 ± 1.8	0.8 ± 0.03	12.4 ± 0.8	15.5 ± 1.1
8	Donor	6.7 ± 0.3	969.1 ± 1336.7	**50.4 ± 6.2****	2158.8 ± 1179.6	6.3 ± 7.5	0.88 ± 0.09	16.3 ± 2.2	18.7 ± 3.5
	Control	7.0 ± 0.0	80.2 ± 35.4	3.2 ± 0.8	13.0 ± 3.1	13.2 ± 1.5	0.79 ± 0.05	11.5 ± 0.6	14.6 ± 0.3
12	Donor	7.0 ± 0.1	**4.0 ± 0.9***	40.2 ± 26	**6905.5 ± 1325.3***	1.6 ± 1.3	1.11 ± 0.19	**26.8 ± 2.3****	**24.5 ± 3.4***
	Control	7.3 ± 0.2	60.3 ± 21.7	3.3 ± 1.8	13.8 ± 4.9	14.0 ± 5.4	0.83 ± 0.14	11.8 ± 2.1	14.3 ± 0.4
16	Donor	**6.7 ± 0.2***	759.1 ± 1307.7	**69.1 ± 12.7***	6377.7 ± 2563.3	1.4 ± 0.8	**1.25 ± 0.03***	**27.0 ± 4.4***	21.7 ± 3.9
	Control	7.3 ± 0.0	69.3 ± 16.1	3.4 ± 0.9	11.1 ± 1.0	12.9 ± 5.9	0.77 ± 0.11	11.5 ± 1.7	14.9 ± 0.3
27	Donor	**6.2 ± 0.3***	706.1 ± 714.1	**87 ± 17.8***	2376.8 ± 1965.3	**1.2 ± 0.7*****	1.62 ± 0.48	28.1 ± 11.4	17.0 ± 2.8
	Control	7.0 ± 0.1	53.2 ± 1.9	7.9 ± 0.8	16.0 ± 2.9	7.0 ± 0.5	0.83 ± 0.24	12.7 ± 4.0	15.2 ± 0.6
43	Donor	**6.1 ± 0.4***	669.4 ± 577.8	**65.5 ± 4.4****	2775.1 ± 1992.2	**0.8 ± 0.4***	1.52 ± 0.33	24.4 ± 5.4	16.6 ± 5.6
	Control	7.0 ± 0.4	98.7 ± 8.5	1.6 ± 0.6	27.4 ± 11.7	9.7 ± 2.2	0.89 ± 0.06	13.1 ± 0.9	14.7 ± 0.1
58	Donor	6.7 ± 0.8	826.9 ± 650.1	**77.1 ± 3.4*****	1492.1 ± 1492.5	**2.0 ± 2.5***	**1.32 ± 0.18***	**19.3 ± 2.5***	14.7 ± 1.2
	Control	7.3 ± 0.0	52.1 ± 21.1	7.3 ± 0.4	12.2 ± 2.1	9.2 ± 0.4	0.87 ± 0.09	13.1 ± 1.7	14.9 ± 0.5
72	Donor	7.0 ± 0.7	**826.0 ± 162.2***	**72.1 ± 7.6****	1679.1 ± 770.7	12.9 ± 11.7	1.09 ± 0.17	14.5 ± 2.6	13.3 ± 1.0
	Control	7.3 ± 0.1	61.8 ± 11.4	2 ± 1.2	8.4 ± 2.1	9.6 ± 4.4	0.83 ± 0.09	11.9 ± 1.4	14.4 ± 0.5
86	Donor	**6.8 ± 0.2***	720.7 ± 422.9	**82.1 ± 24***	1895.2 ± 2108.3	41.0 ± 35.9	1.32 ± 0.41	20.8 ± 7.5	15.6 ± 1.2
	Control	7.3 ± 0.1	50.5 ± 26.3	4.5 ± 1.4	11.6 ± 4.7	13.7 ± 8.6	0.81 ± 0.08	11.7 ± 1.1	14.4 ± 0.1
103	Donor	6.6 ± 0.4	572.9 ± 393.8	57.8 ± 33.6	470.7 ± 294.5	112.4 ± 77.2	**1.22 ± 0.17***	15.9 ± 3.3	13.0 ± 1.1
	Control	7.0 ± 0.4	49.7 ± 8.9	3.4 ± 0.9	10.7 ± 1.8	9.8 ± 3.4	0.8 ± 0.16	11.8 ± 2.7	14.8 ± 0.4
117	Donor	6.5 ± 0.6	488.5 ± 225	35.4 ± 18.7	431.1 ± 534.0	186.1 ± 156.8	**1.09 ± 0.05***	13.7 ± 0.9	12.5 ± 0.9
	Control	7.0 ± 0.3	35.0 ± 14.5	2 ± 0.6	12.6 ± 6.1	11.7 ± 3.9	0.75 ± 0.11	10.4 ± 1.7	13.9 ± 0.2
132	Donor	**6.1 ± 0.3***	552.5 ± 297	29.2 ± 36	366.9 ± 367.4	**203.6 ± 65.2***	**1.04 ± 0.05***	12.4 ± 0.9	**12.0 ± 0.7***
	Control	6.9 ± 0.2	78.4 ± 34.9	1.8 ± 0.7	5.6 ± 0.7	13.5 ± 3.3	0.74 ± 0.13	10.6 ± 2.4	14.1 ± 0.8
150	Donor	**6.3 ± 0.4***	497.3 ± 240.6	22.9 ± 8.9	**267.1 ± 77.2***	**129.6 ± 46.4***	1.15 ± 0.21	13.8 ± 2.2	12.1 ± 0.5
	Control	7.2 ± 0.1	44.3 ± 11	4.8 ± 1.7	10.1 ± 3.2	7.9 ± 0.7	0.95 ± 0.31	12.7 ± 3.6	13.6 ± 1.9
168	Donor	5.8 ± 0.7	**547.7 ± 183.3***	20.5 ± 16.5	371.9 ± 271.6	220.5 ± 116.5	1.5 ± 0.75	15.2 ± 5.1	10.7 ± 1.8
	Control	7.2 ± 0.2	44.5.0 ± 14	3.5 ± 0.2	9.4 ± 3.3	8.4 ± 2.5	0.76 ± 0.15	11.2 ± 3.5	14.5 ± 1.8
201	Donor	**5.8 ± 0.5***	**289.6 ± 54.8***	19.6 ± 14.2	282.7 ± 205.1	116.5 ± 47.4	**1.14 ± 0.15***	13.2 ± 1.6	**11.6 ± 0.9***
	Control	7.2 ± 0.1	50.4 ± 9.5	4.6 ± 0.9	8.6 ± 1.2	7.4 ± 0.9	0.74 ± 0.15	10.7 ± 2.9	14.4 ± 1.0
254	Donor	6.5 ± 1.2	**514.7 ± 178.7***	21.7 ± 18.7	775.8 ± 331.5	195.7 ± 186.4	1.05 ± 0.24	11.6 ± 1.8	**11.2 ± 1.1***
	Control	7.6 ± 0.1	58.6 ± 22.2	5.8 ± 2.1	9.9 ± 2.1	10.0 ± 1.0	0.82 ± 0.19	12.4 ± 2.7	15.2 ± 0.4
303	Donor	6.9 ± 0.8	516.5 ± 499.7	24.2 ± 11.9	1202.0 ± 1211.5	176.3 ± 136.9	1.03 ± 0.3	12.0 ± 3.0	**11.7 ± 0.5***
	Control	7.3 ± 0.1	40.2 ± 5.3	6.3 ± 1.5	9.0 ± 1.2	6.9 ± 0.6	0.77 ± 0.18	11.3 ± 3.2	14.5 ± 0.9
340	Donor	6.0 ± 0.6	431.3 ± 245.6	17.1 ± 9.9	476.5 ± 414.0	189.3 ± 169.9	**1.15 ± 0.01***	13.4 ± 0.6	**11.7 ± 0.6***
	Control	7.2 ± 0.0	75.4 ± 6.2	6.8 ± 2.6	10.0 ± 3.7	11.1 ± 1.4	0.86 ± 0.1	13.2 ± 2.6	15.3 ± 1.4
357	Donor	**5.9 ± 0.1*****	187.3 ± 126.4	11.7 ± 3.7	314.8 ± 362.7	186.8 ± 216.9	1.1 ± 0.12	12.6 ± 1.8	**11.5 ± 0.4****
	Control	6.7 ± 0.1	42.9 ± 5.8	8.1 ± 1.5	10.4 ± 1.8	9.9 ± 0.7	0.73 ± 0.21	10.7 ± 3.2	14.8 ± 0.6
376	Donor	5.8 ± 0.8	165.6 ± 215.8	8.2 ± 2.8	132.6 ± 183.6	63.3 ± 88.3	0.89 ± 0.07	11.8 ± 0.7	13.4 ± 1.6
	Control	7.3 ± 0.4	34.5 ± 3.6	4.2 ± 1.4	6.7 ± 1.0	7.4 ± 2.3	0.81 ± 0.29	12.8 ± 2.6	16.9 ± 5.1

Data for pH, EC, respiration, ammonium, nitrate, total N (%N), total C (%C), and the C:N ratio are shown for decomposition (donor) and control soils. Respiration, ammonium, and nitrate data are represented as per gram dry weight of soils (gdw). Data are means ± standard deviations for $n = 3$ replicate donors. Impacted soils that significantly differ from controls based upon Welch t-tests ($P < .05$) are presented in bold type. Data are means ± standard deviations for $n = 3$ replicate donors. Asterisks indicate levels of significance: *$P < .05$, **$P < .01$, and ***$P < .001$.

Table 5. Winter 2019 soil chemical parameters in core soils (1–16 cm).

Study day	Location	pH	EC ($\mu S\ cm^{-1}$)	DO (%)	Respiration ($\mu mol\ CO_2\ gdw^{-1}\ day^{-1}$)	Ammonium ($\mu g\ gdw^{-1}$)	Nitrate ($\mu g\ gdw^{-1}$)	%N	%C	C:N
0	Donor	7.6 ± 0.1	52.4 ± 14.4	103 ± 1	2.1 ± 0.3	9.2 ± 0.9	5.9 ± 1.0	0.54 ± 0.18	7.5 ± 1.8	14.1 ± 1.4
	Control	7.6 ± 0.1	53.2 ± 8.6	101.6 ± 1.2	2 ± 0.5	9.0 ± 0.4	6.6 ± 2.1	0.6 ± 0.19	8.1 ± 1.7	13.8 ± 1.4
21	Donor	7.4 ± 0.1	114.6 ± 43.9	97 ± 1.5	3 ± 1.2	21.2 ± 12.0	25.6 ± 13.9	0.54 ± 0.22	7.0 ± 2.4	13.3 ± 1.1
	Control	7.6 ± 0.2	73.1 ± 16.0	98.9 ± 0.7	2.6 ± 0.3	9.0 ± 1.4	9.6 ± 0.6	0.62 ± 0.15	8.6 ± 2.3	14.0 ± 1.5
38	Donor	7.3 ± 0.2	**193.2 ± 56.7***	101.3 ± 1.9	**19.3 ± 1.6****	**160.7 ± 22.1****	24.9 ± 18.6	0.61 ± 0.19	8.1 ± 2.3	13.3 ± 0.4
	Control	7.6 ± 0.1	49.1 ± 9.9	102.8 ± 0.8	2.3 ± 0.1	9.1 ± 1.2	8.9 ± 1.4	0.63 ± 0.2	8.3 ± 2.1	13.4 ± 1.0
55	Donor	7.3 ± 0.2	246.9 ± 90.5	**89.1 ± 4.3***	**34.6 ± 8***	215.3 ± 171.7	44.1 ± 20.8	0.63 ± 0.11	8.4 ± 0.8	13.5 ± 1.2
	Control	7.8 ± 0.2	47.8 ± 13.0	99.6 ± 0.6	2.7 ± 0.5	7.3 ± 2.1	11.7 ± 0.9	0.59 ± 0.12	8.4 ± 2.6	14.2 ± 1.6
75	Donor	7.1 ± 0.5	**218.4 ± 41.3***	**71.3 ± 8.4***	**30.9 ± 2*****	231.4 ± 186.4	12.7 ± 10.1	0.68 ± 0.23	9.1 ± 2.1	13.7 ± 1.4
	Control	7.4 ± 0	45.8 ± 5.4	100.1 ± 1.3	2.8 ± 0.7	7.4 ± 0.4	8.3 ± 2.9	0.75 ± 0.18	10.7 ± 2.6	14.3 ± 1.8
94	Donor	**6.5 ± 0.1****	235.4 ± 81.8	74.8 ± 30.9	26.7 ± 11.2	**190.9 ± 17.5****	25.4 ± 21.6	0.59 ± 0.21	7.8 ± 2.1	13.7 ± 2.2
	Control	7.5 ± 0	39.4 ± 4.4	101.9 ± 0.5	2.9 ± 2.3	7.7 ± 3.3	6.3 ± 1.29	0.68 ± 0.25	9.5 ± 3.9	13.8 ± 0.8
110	Donor	6.4 ± 0.3	356.4 ± 184.9	86.8 ± 9.2	33.5 ± 20.3	230.8 ± 240.3	32.3 ± 39.5	0.69 ± 0.12	9.8 ± 1.0	14.4 ± 2.3
	Control	7.2 ± 0.5	41.4 ± 17.9	101.1 ± 0.9	1.4 ± 0.3	7.3 ± 0.8	9.4 ± 4.1	0.62 ± 0.18	9.0 ± 3.1	14.5 ± 0.9
126	Donor	6.6 ± 0.4	245.4 ± 129.4	97.2 ± 3.8	**21.8 ± 4.6***	163.9 ± 62.9	**62.6 ± 16.9***	0.68 ± 0.12	9.5 ± 0.9	14.1 ± 1.7
	Control	7.3 ± 0.2	62.6 ± 6.3	101.1 ± 1.1	1.6 ± 0.4	7.9 ± 0.9	17.8 ± 4.3	0.62 ± 0.13	8.4 ± 1.3	13.7 ± 1.0
140	Donor	**6.6 ± 0.2***	214.0 ± 96.0	90.7 ± 9.9	17.6 ± 6.6	329.4 ± 210.5	75.1 ± 48.9	0.75 ± 0.14	9.8 ± 1.0	13.2 ± 1.2
	Control	7.4 ± 0.2	46.7 ± 10.0	100.7 ± 0.5	2 ± 0.2	9.3 ± 1.2	10.2 ± 2.4	0.53 ± 0.17	7.6 ± 2.2	14.4 ± 0.7
158	Donor	**6.3 ± 0.3***	211.9 ± 109.1	92 ± 11	18.1 ± 17.2	185.5 ± 176.0	**60.7 ± 19.3***	0.81 ± 0.25	10.7 ± 3.2	13.4 ± 1.6
	Control	7.4 ± 0.1	40.5 ± 8.5	100.5 ± 0.5	1.8 ± 0.4	7.6 ± 2.1	8.5 ± 1.2	0.58 ± 0.13	7.9 ± 1.5	13.8 ± 1.0
172	Donor	**6.4 ± 0.2***	**236 ± 46.6***	97.4 ± 3.7	18.4 ± 22	155.0 ± 155.2	67.0 ± 78.7	1.18 ± 1.05	12.0 ± 9.1	11.1 ± 1.7
	Control	7.2 ± 0.3	31.3 ± 4.7	100.3 ± 0.7	1.4 ± 0.3	7.3 ± 1.7	7.8 ± 2.5	0.52 ± 0.33	6.9 ± 4.1	13.6 ± 1.3
186	Donor	**6.9 ± 0.2***	180.0 ± 74.8	98.6 ± 4.1	**7.3 ± 2.1***	39.8 ± 18.6	40.7 ± 39.6	0.48 ± 0.16	6.1 ± 1.8	12.6 ± 0.9
	Control	7.3 ± 0.2	36.4 ± 3.7	101.3 ± 0.2	1 ± 0.1	4.8 ± 0.8	2.7 ± 1.2	0.57 ± 0.27	8.3 ± 3.8	14.4 ± 1.9
201	Donor	7.1 ± 0.3	154.7 ± 17.4	100.2 ± 1	5.8 ± 4.5	12.2 ± 6.9	23.8 ± 9.4	0.69 ± 0.35	9.2 ± 5.0	13.1 ± 0.6
	Control	7.3 ± 0.1	95.6 ± 80	100.9 ± 0.1	2.4 ± 2.2	10.6 ± 10.1	27.4 ± 30.7	0.53 ± 0.13	6.8 ± 0.8	13.0 ± 1.6
216	Donor	6.8 ± 0.2	114.7 ± 47.3		1.8 ± 0.9	32.7 ± 24.5	36.3 ± 34.8	0.49 ± 0.28	5.9 ± 3.3	12.2 ± 0.4
	Control	7.2 ± 0.3	36.2 ± 9.8		0.5 ± 0.1	6.1 ± 0.7	7.6 ± 2.7	0.52 ± 0.17	7.0 ± 1.8	13.7 ± 1.1
234	Donor	**6.7 ± 0.2***	250.7 ± 276.9		1.3 ± 0.6	64.3 ± 74.9	61.4 ± 69.9	0.72 ± 0.25	9.0 ± 3.0	12.6 ± 0.8
	Control	7.2 ± 0.1	32 ± 6.3		0.4 ± 0	6.5 ± 1.8	12.3 ± 2.6	0.62 ± 0.1	8.3 ± 1.3	13.5 ± 1.1
252	Donor	**6.9 ± 0.1***	185.1 ± 130.2		**3.4 ± 0.3****	36.9 ± 18.9	58.6 ± 40.5	0.51 ± 0.26	6.1 ± 2.8	12.2 ± 0.6
	Control	7.1 ± 0.1	90.7 ± 7.1		1.7 ± 0.3	6.6 ± 2.3	27.6 ± 10.4	0.54 ± 0.1	7.1 ± 1.5	13.1 ± 1.0
290	Donor	7.1 ± 0.2	103.3 ± 84.2		**4.7 ± 1.1***	16.8 ± 12.5	34.4 ± 31.9	0.6 ± 0.19	7.7 ± 2.1	13.0 ± 1.8
	Control	7.4 ± 0	43.1 ± 3.5		1.3 ± 0.1	4.8 ± 0.6	5.1 ± 2.7	0.55 ± 0.11	7.1 ± 1.3	13.0 ± 0.5
335	Donor	**7.0 ± 0.2***	98.7 ± 63.0		**5.8 ± 1.5***	43.8 ± 60.4	38.8 ± 41.2	0.64 ± 0.38	7.2 ± 3.6	11.7 ± 1.0
	Control	7.6 ± 0	46.5 ± 3.8		2.1 ± 0.6	3.6 ± 0.9	7.2 ± 1.7	0.62 ± 0.1	8.0 ± 1.5	12.9 ± 0.9
384	Donor	6.8 ± 0.3	133.3 ± 137.0		**7 ± 2.2***	13.9 ± 13.2	21.8 ± 17.9	0.76 ± 0.21	9.1 ± 2.9	11.9 ± 0.9
	Control	7.4 ± 0	53.6 ± 22.0		1.5 ± 0.4	5.6 ± 1.1	7.3 ± 1.2	0.51 ± 0.19	6.9 ± 2.2	13.7 ± 0.9

Data for pH, EC, DO, respiration, ammonium, nitrate, total N (%N), total C (%C), and the C:N ratio are shown for decomposition (donor) and control soils. Respiration, ammonium, and nitrate data are represented as per gram dry weight of soils (gdw). Data are means ± standard deviations for $n = 3$ replicate donors. Impacted soils that significantly differ from controls based upon Welch t-tests ($P < .05$) are presented in bold type. Data are means ± standard deviations for $n = 3$ replicate donors. Asterisks indicate levels of significance: *$P < .05$, **$P < .01$, and ***$P < .001$.

similar manner to spring core soils patterns of change were not noteworthy.

Winter 2019 interface (0–1 cm) samples. As observed in spring trial, all interface soil chemical parameters differed significantly from control soils (Kruskal–Wallace, $P < .05$) (Supplementary file 1: Table S6). Overall patterns followed those of winter cores with respect to timing, and with the exception of pH, parameter maxima (or minima) occurred during active and early advanced decay (days 55–94) (Figs 1 and 2, Table 6; Supplementary file 1: Table S7). pH became more acidic, reaching 6.2 ± 0.2 mid-way through skeletonization (day 216; 104 845 ADH). Respiration rates increased during active decay (day 38; 7594 ADH), reaching a maximum in early advanced decay (day 94; 33 575 ADH) of 97.5 ± 7.7 μmol CO_2 gdw^{-1} day^{-1}, and remained elevated throughout much of the study. Mean EC and ammonium concentrations both reached their maxima during active decay (day 55; 12 127 ADH) at 926.8 ± 576.7 μS cm^{-1} and 2811.2 ± 2241.2 μg gdw^{-1}. TC, TN, and the C:N ratio patterns followed those observed for spring interface soils: simultaneous maxima of TC and TN (day 94), early recovery of TC (day 110, 43 005 ADH), late elevations of TN (day 335, 142 473 ADH), and C:N patterns that were initially elevated above controls and fell below control values during the latter half of the study. As observed in the spring trial nitrate concentrations fell below control concentrations early in the study (days 38–94), although in this case reductions in concentration occurred simultaneously with ammonium concentration increases and just prior to oxygen decreases.

Fungal communities

Diversity and abundances

Fungal community alpha diversity (Shannon, Inverse Simpson, and Chao1) decreased during the onset of soil chemical changes and remained low for the remainder of both study trials (Kruskal–Wallace, $P < .05$) (Supplementary file 1: Tables S8–S11). The opposite effect was observed for fungal gene copy number, and the fungal:bacterial ratio (Kruskal–Wallace, $P < .05$) (Supplementary file 1: Tables S8–S11). The decrease in alpha diversity occurred earlier in the spring trial in comparison with the winter trial, and depth effects were not noticeably present (Fig. 3). In contrast, increases in fungal gene copy number and the fungal:bacterial ratio occurred early in advanced decay during both spring and winter, with greater effects observed in interface soils (Fig. 3, Tables 7 and 8; Supplementary file 1: Tables S8–S11).

CAP coordinates of Bray–Curtis distances and PERMANOVA showed significant differences in community structure between controls and impacted soils by study day ($P < .001$) (Fig. 4). Community changes during early decomposition are positively correlated with increases in ammonium (NH_4), TC, TN, CN ratio, EC, fungal gene abundances, and the fungal:bacterial ratio, and negatively correlated to pH and soil oxygen (DO). Later communities correlated with increased concentrations of nitrate (NO_3) (Fig. 4). This same pattern was observed for the winter trial, however communities exhibited greater dispersion. In both trials community structure remained altered compared with initial communities by the end of 1 year.

Community composition

Spring 2018: of phyla representing greater than 2% relative abundance in spring trial soils, *Ascomycota* constituted the largest proportion of community composition in all control samples of both soil depths, followed by *Basidiomycota*, *Mortierellomycota*, *Mucoromycota*, and *Rozellomycota* (Supplementary file 1: Fig. S6). From bloat through early advanced decay (days 8–58) in interfaces, community composition became almost exclusively composed of *Ascomycota*, specifically *Yarrowia* (Supplementary file 2); this shift occurred simultaneously with decreases in pH, soil oxygen, and nitrate concentrations, and peak elevations of EC, respiration rates, and ammonium concentrations (Supplementary file 1:Fig. S6; Fig. 4). During this same period, soil temperatures remained consistently elevated above 30°C and fly larvae were present. Similar community shifts were observed in cores, although over a shorter period of time (days 12–43). At the class-level, dominant members were *Saccharomycetes* and *Sordariomycetes* (both *Ascomycota*) (Fig. 5; Supplementary file 1: Fig. S7). Relative abundances of *Saccharomycetes*, primarily composed of *Yarrowia*, increased during the period of elevated respiration and reduced soil oxygen in both cores and interfaces. During the *Saccharomycetes* bloom, *Sordariomycetes* decreased to <15% relative abundance in interfaces then began to increase after day 27 and by the end of the study constituted 50% relative abundance. In contrast, in core samples *Sordariomycetes* increased in conjunction with *Saccharomycetes*, and following day 16 composed 30%–40% of sample abundance for the remainder of the study. At both depths *Sordariomycetes* increases were driven in large part by the genus *Scedosporium*, which frequently constituted >20% of the sample relative abundance (Supplementary file 2). *Tremellomycetes* (*Basidiomycota*), below the detection cutoff in initial samples, also increased beginning in early advanced decay (day 27), peaking between days 86 and 117 in both soil depths. Decreased relative abundances were also observed for *Eurotiomycetes* (*Ascomycota*), *Agaricomycetes*, and *Archaeorhizomycetes* (*Ascomycota*); *Agaricomycetes* and *Eurotiomycetes* recovered to initial proportions while the others remained low. Community structures were still impacted at the end of the study, notably with increased relative abundances of *Sordariomycetes* in both soil depths in comparison with control samples.

Winter 2019: changes in phyla, classes, and genera during the winter trial were broadly similar to those found in the spring trial, i.e. an early *Saccharomycetes* bloom, followed by later increases in *Sordariomycetes*. However, both timings and magnitudes of taxon changes followed seasonally dependent patterns of decomposition progression and their reflections in soil chemistry, thus winter trial taxon changes were less pronounced and their abundances were less clearly defined due to slow seepage of decomposition products into the soil (Supplementary file 1: Figs S8 and S9; Figs 4 and 5). *Saccharomycetes* abundances increased in both soil depths in early advanced decay (day 75, ADD 822), much later than the increase observed during the bloat stage of the spring trial (day 8, ADD 164). *Tremellomycetes* increased earlier during the winter trial, as early as active decay (day 38) in cores, and during the *Saccharomycetes* bloom, rather than following it as observed in the spring (Supplementary file 1: Fig. S9). Notably, *Scedoscorium* relative abundance increases following the brief *Yarrowia* bloom were commensurate with those observed in the spring study for both soil depths (Supplementary file 2).

Bacterial communities

Diversity and abundances

As with fungal communities, all bacterial alpha diversity metrics decreased with soil chemical changes in the spring relative to controls, however only Shannon diversity and Chao1 significantly changed in the winter trial (Kruskal–Wallace, $P <$ .05) (Supplementary file 1: Tables S8–S11). Bacterial gene copy abundances did not differ between decomposition impacted soils and controls in spring cores (Kruskal–Wallace, $P < .05$)

Table 6. Winter 2019 soil chemical parameters in interface soils (0–1 cm).

Study day	Location	pH	Conductivity ($\mu S\ cm^{-1}$)	Respiration ($\mu mol\ CO_2\ gdw^{-1}\ day^{-1}$)	Ammonium ($\mu g\ gdw^{-1}$)	Nitrate ($\mu g\ gdw^{-1}$)	%N	%C	C:N
0	Donor	7.4 ± 0.2	64.5 ± 25.1	6.5 ± 1	7.2 ± 1.6	5.7 ± 1.0	0.94 ± 0.05	15.0 ± 0.2	16.1 ± 0.9
	Control	7.4 ± 0.2	52.8 ± 4.1	7.4 ± 3.4	13.2 ± 10.4	7.3 ± 1.6	0.99 ± 0.18	15.9 ± 3.4	16.2 ± 2.3
21	Donor	7.2 ± 0.1	90.9 ± 19	19 ± 6.4	35.6 ± 27.4	16.7 ± 17.7	0.91 ± 0.15	13.3 ± 1.9	14.6 ± 0.4
	Control	7.4 ± 0.1	67.6 ± 7.5	6.6 ± 1.4	21.3 ± 18.9	9.1 ± 1.9	0.88 ± 0.18	13.4 ± 3.2	15.2 ± 1.1
38	Donor	7.2 ± 0.2	621.8 ± 321.6	**73.3 ± 5.6*** **	**2162.2 ± 769.9***	**1.8 ± 1.8***	1.13 ± 0.06	17.5 ± 3.4	15.4 ± 2.8
	Control	7.4 ± 0.2	54.2 ± 14.7	6.8 ± 2.7	11.5 ± 5.0	12.4 ± 3.1	1.01 ± 0.18	15.4 ± 3.0	15.4 ± 2.0
55	Donor	7.1 ± 1.0	926.8 ± 576.7	**93.7 ± 9.8****	2811.2 ± 2241.2	**0.7 ± 0.4***	1.31 ± 0.54	21.9 ± 2.3	18.4 ± 6.0
	Control	7.4 ± 0.4	72.0 ± 55.7	7.7 ± 2.9	16.7 ± 14.4	15.5 ± 4.4	0.92 ± 0.13	15.1 ± 4.6	16.3 ± 3.6
75	Donor	6.9 ± 0.6	496.1 ± 476.6	**89 ± 20***	2639.8 ± 3859.4	18.2 ± 28.5	1.27 ± 0.32	20.1 ± 5.5	16.2 ± 5.4
	Control	7.2 ± 0.1	59.2 ± 12.7	7.4 ± 2.7	12.5 ± 3.8	10.7 ± 1.0	0.87 ± 0.12	12.8 ± 0.9	14.9 ± 1.3
94	Donor	**7.1 ± 0.1***	**512.6 ± 153.1***	**97.5 ± 7.7****	**1910.2 ± 268.2****	**0.7 ± 0.3****	1.72 ± 0.41	**27.3 ± 5.2***	16.0 ± 1.0
	Control	7.4 ± 0.0	38.3 ± 9.8	3.5 ± 1.4	7.7 ± 2.2	7.0 ± 1.1	0.85 ± 0.16	12.3 ± 1.1	14.7 ± 1.6
110	Donor	**6.3 ± 0.2****	**532.1 ± 172.6***	77.9 ± 35.8	624.0 ± 354.4	42.9 ± 24.4	1.38 ± 0.30	20.6 ± 5.7	15.0 ± 3.1
	Control	7.4 ± 0.2	47.7 ± 19.6	1.3 ± 0.6	12.7 ± 4.0	18.7 ± 8.7	0.82 ± 0.15	11.5 ± 1.5	14.1 ± 0.9
126	Donor	6.7 ± 0.3	465.6 ± 218.9	**83.6 ± 23.2***	1250.7 ± 1058.9	66.1 ± 51.4	1.72 ± 0.55	22.9 ± 9.9	13.1 ± 1.5
	Control	7.3 ± 0.2	44.0 ± 1.4	4.3 ± 2.5	11.0 ± 4.3	15.7 ± 3.0	0.85 ± 0.17	13.4 ± 3.9	15.7 ± 2.6
140	Donor	7.0 ± 0.3	**288.6 ± 67.8***	**73.8 ± 2.9*****	992.3 ± 628.7	82.0 ± 89.8	1.29 ± 0.26	18.3 ± 4.2	14.3 ± 2.8
	Control	7.3 ± 0.4	46.6 ± 15.8	3.4 ± 1	10.8 ± 4.6	12.9 ± 5.8	0.84 ± 0.12	12.8 ± 0.7	15.4 ± 1.8
158	Donor	6.9 ± 0.5	**369.7 ± 52.5****	**67.8 ± 4.7****	**607.1 ± 42.6****	142.5 ± 132.5	1.51 ± 0.37	18.0 ± 2.8	12.1 ± 1.4
	Control	7.6 ± 0.1	49.0 ± 2.7	3.7 ± 0.9	11.7 ± 4.7	12.2 ± 1.4	0.89 ± 0.09	14.2 ± 3.1	15.9 ± 2.7
172	Donor	**6.5 ± 0.4***	237.6 ± 104.7	46.7 ± 33.7	371.8 ± 288.9	137.8 ± 153.7	1.18 ± 0.3	15.4 ± 5.0	12.9 ± 1.1
	Control	7.4 ± 0.2	31.5 ± 3.4	1.4 ± 0.1	6.8 ± 0.2	13.9 ± 4.8	0.84 ± 0.23	12.8 ± 4.3	15.2 ± 3.0
186	Donor	**6.4 ± 0.1****	243.3 ± 94.6	**9.7 ± 2.3***	302.0 ± 182.9	127.4 ± 46.2	1.08 ± 0.19	13.4 ± 2.6	12.3 ± 0.5
	Control	7.4 ± 0.2	34.6 ± 14.5	0.5 ± 0.1	7.7 ± 1.4	13.7 ± 2.0	0.79 ± 0.07	11.4 ± 0.4	14.4 ± 1.1
201	Donor	6.6 ± 0.5	347.2 ± 322.8	**24.3 ± 4.2****	345.4 ± 264.8	140.0 ± 166.1	1.42 ± 0.36	16.1 ± 4.7	11.2 ± 1.1
	Control	7.6 ± 0.2	67.9 ± 16.6	3.5 ± 1.2	7.9 ± 4.1	11.0 ± 0.4	0.88 ± 0.03	13.5 ± 1.6	15.4 ± 2.3
216	Donor	**6.2 ± 0.2****	**268.9 ± 89.3***	2.1 ± 0.7	211.7 ± 196.7	241.3 ± 140.0	1.19 ± 0.22	14.7 ± 2.8	12.3 ± 0.5
	Control	7.4 ± 0.1	45.2 ± 4.8	0.3 ± 0	12.8 ± 0.3	13.0 ± 2.5	0.83 ± 0.03	11.9 ± 0.9	14.4 ± 1.4
234	Donor	6.3 ± 0.4	199.5 ± 140.7	0.9 ± 0.5	168.5 ± 107.8	143.5 ± 93.7	1.07 ± 0.18	13.0 ± 1.6	12.2 ± 0.7
	Control	7.0 ± 0.2	75.0 ± 14.1	0.4 ± 0.2	18.4 ± 8.0	35.0 ± 16.0	0.87 ± 0.17	13.3 ± 3.1	15.4 ± 2.5
252	Donor	**6.5 ± 0.1****	201.4 ± 95.0	**11.1 ± 2.3***	225.6 ± 139.6	195.0 ± 80.7	1.14 ± 0.67	13.3 ± 5.9	12.2 ± 1.5
	Control	7.3 ± 0.0	96.1 ± 36.7	3.4 ± 0.5	6.0 ± 1.6	30.3 ± 9.1	0.73 ± 0.10	10.3 ± 0.7	14.3 ± 1.2
290	Donor	6.6 ± 0.4	211.1 ± 207.6	**10.8 ± 2.5***	113.8 ± 129.4	108.7 ± 121.0	0.89 ± 0.01	11.2 ± 1.2	12.5 ± 1.2
	Control	7.2 ± 0.1	51.2 ± 12.4	2.8 ± 0.4	8.8 ± 2.6	5.6 ± 0.50	0.7 ± 0.08	9.7 ± 0.7	14.0 ± 1.0
335	Donor	**6.7 ± 0.3***	140.5 ± 82.5	**16.4 ± 4.2***	30.2 ± 13.2	78.1 ± 42.6	**1.03 ± 0.02***	12.3 ± 1.6	11.9 ± 1.3
	Control	7.5 ± 0.0	45.9 ± 9.7	4.3 ± 0.4	4.5 ± 0.9	7.7 ± 1.8	0.78 ± 0.07	11.1 ± 0.5	14.3 ± 0.9
384	Donor	6.6 ± 0.4	156.9 ± 120.0	21 ± 10.6	176.9 ± 259.7	81.8 ± 69.4	**1.17 ± 0.17***	13.6 ± 2.3	11.7 ± 1.6
	Control	6.9 ± 0.3	47.8 ± 6.7	4.3 ± 2.3	34.2 ± 44.6	7.1 ± 1.2	0.72 ± 0.09	10.6 ± 1.0	14.9 ± 0.7

Data for pH, EC, respiration, ammonium, nitrate, total N (%N), total C (%C), and the C:N ratio are shown for decomposition (donor) and control soils. Respiration, ammonium, and nitrate data are represented as per gram dry weight of soils (gdw). Data are means ± standard deviations for $n = 3$ replicate donors. Impacted soils that significantly differ from controls based upon Welch t-tests ($P < .05$) are presented in bold type. Data are means ± standard deviations for $n = 3$ replicate donors. Asterisks indicate levels of significance: *$P < .05$, **$P < .01$, and ***$P < .001$.

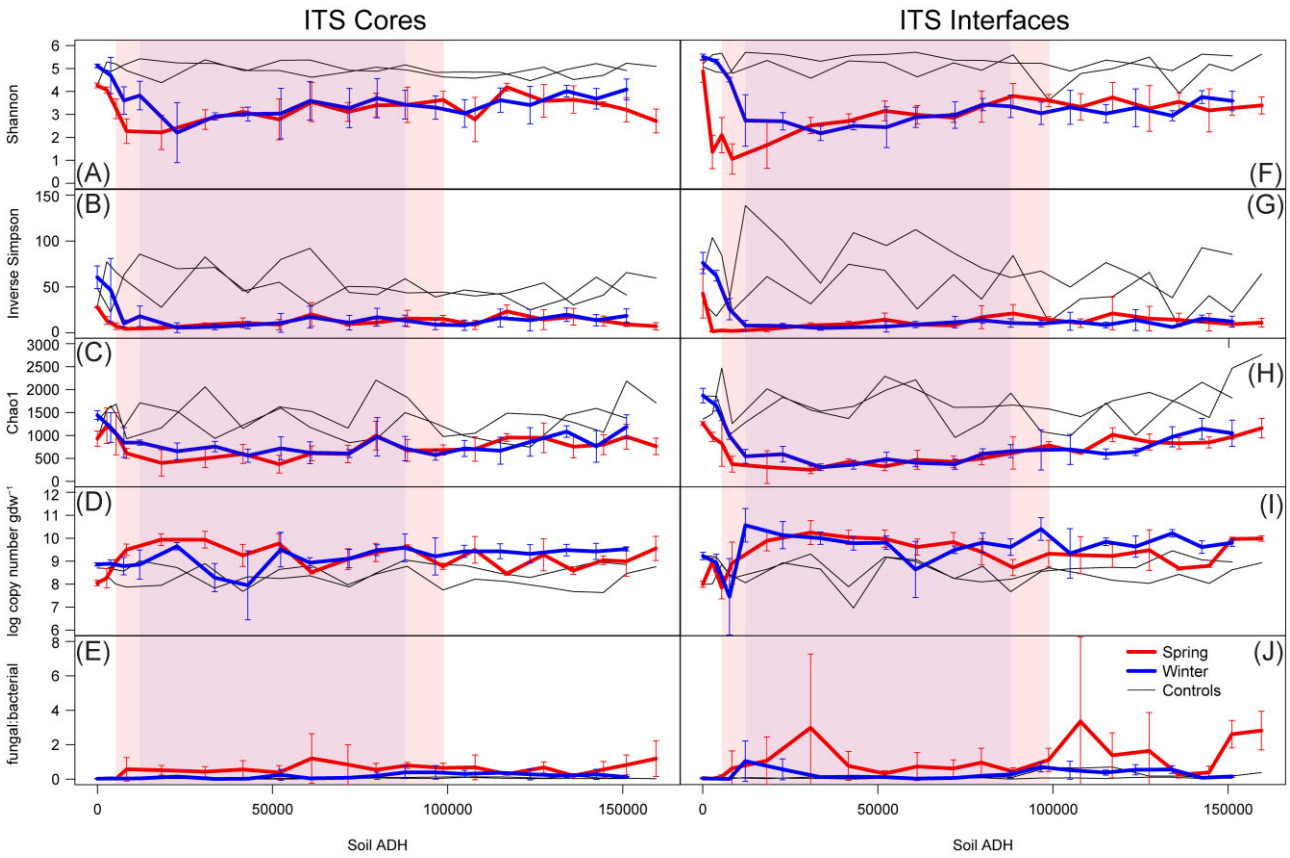

Figure 3. Seasonal comparisons in fungal diversity in core and interface soils. The magnitude and timing of changes in (A and F) the Shannon index, (B and G) the Inverse Simpson index, (C and H) the Chao1 index, (D and I) log of gene copy number, and (E and J) the fungal:bacterial gene copy ratio in core (1–16 cm) and interface (0–1 cm) soils are presented in units of equivalent thermal units based upon soil temperatures (soil ADH). Data is based on internal transcribed spacer (ITS) sequences of fungal rRNA genes, and abundance data was calculated based on fungal gene copy numbers determined by qPCR. Means and standard deviations are shown for samples ($n = 3$). Controls for each time point were pooled. Shaded areas correspond to periods of reduced soil oxygen for the spring (lighter shading) and winter (darker shading).

(Supplementary file 1: Tables S8–S11). Alpha diversity differences between controls and decomposition soils were pronounced in interfaces, however little difference was observed in core soils throughout both seasonal studies (Fig. 6). Changes in bacterial gene copy abundances were negligible (Fig. 6, Tables 7 and 8; Supplementary file 1: Tables S8–S11).

In both trials, CAP results demonstrated significant bacterial community structure changes throughout the entire decomposition process, and that recovery to initial conditions appeared to partially occur in core soils by the final sampling time point of each trial (Fig. 7). Bacterial community structure changes during early decomposition were positively correlated with increases in ammonium (NH_4), TC, TN, CN ratio, EC, and negatively correlated to pH and soil oxygen (DO), whereas later community changes are correlated with increased concentrations of nitrate (NO_3) (Fig. 7).

Community composition

Spring 2018: phyla that were the greatest contributors to relative abundance in control soils were *Proteobacteria*, *Actinobacteria*, and *Acidobacteria* (Supplementary file 1: Fig. S10). In decomposition soils, *Firmicutes* relative abundances increased from bloat through early advanced decay (days 8–103) in both soil depths, concomitant with reduced soil oxygen and decreases in *Proteobacteria*. Following day 43, relative abundances of *Bacteroidetes* and *Proteobacteria* increased and *Actinobacteria* decreased at both sample depths. *Acidobacteria* relative abundances decreased in interfaces during bloat and remained low for the remainder of the trial. At the class level, *Clostridia* (*Firmicutes*) increased in impacted interface soils from days 8 to 43, commensurate with reduced pH and soil oxygen and increased abundances of *Saccharomycetes (Yarrowia)* fungi (Fig. 8; Supplementary file 1: Fig. S11). Also during this time (days 8–16), a brief increase in *Gammaproteobacteria* was observed in interfaces, partially composed of the genus *Ignatzschineria* (16% relative abundance), which is frequently associated with the presence of blow-flies (Supplementary file 2). Following day 43 *Gammaproteobacteria* and *Bacteroidia* (*Bacteroidetes*) increased in both soil depths; *Gammaproteobacteria* remained enriched for the remainder of the trial, however *Bacteroidia* abundances declined in the final two sampling time points to approximately baseline values. Relative abundances of *Actinobacteria* increased in both soil depths following day 27, remaining elevated for the remainder of the trial, and composing 20%–30% of relative abundances in interfaces. *Alphaproteobacteria* (*Proteobacteria*) relative abundances decreased in interfaces during *Clostridia* enrichment, but recovered by day 58, although no discernable change occurred in core soils. *Verrucomicrobiae* (*Verrucomicrobia*) and *Thermoleophilia* (an *Actinobacteria*) abundances also decreased during the *Clostridia* bloom, and abundances remained low throughout the remainder of the study. Following the *Clostridia* bloom (day 58, mid-advanced decay) community composition at the class level changed only gradually, and by the end of the study differences from initial communities were largely attributable to increased

Table 7. Spring 2018 microbial abundances in interface (0–1 cm) and core (1–16 cm) soils.

Depth		Interface			Core		
Study day	Location	16S copy numbers (log copies gdw^{-1})	ITS copy numbers (log copies gdw^{-1})	Fungal:bacterial ratio	16S copy numbers (log copies gdw^{-1})	ITS copy numbers (log copies gdw^{-1})	Fungal:bacterial ratio
0	Donor	9.22 ± 0.08	**8 ± 0.13****	**0.061 ± 0.009***	9.69 ± 0.09	8.05 ± 0.12	**0.025 ± 0.013***
	Control	9.27	7.99	0.053	9.65	7.92	0.019
8	Donor	**10.64 ± 0.1*****	**8.99 ± 0.16****	**0.023 ± 0.009****	9.81 ± 0.56	8.26 ± 0.42	0.033 ± 0.023
	Control	9.36	8.02	0.046	9.76	8.37	0.041
12	Donor	8.88 ± 0.88	7.85 ± 0.49	0.131 ± 0.124	**10.57 ± 0.09*****	**8.98 ± 0.09*****	**0.026 ± 0.004****
	Control	10.3	8.86	0.036	10.33	8	0.005
16	Donor	9.76 ± 0.47	8.92 ± 0.91	0.624 ± 1.007	10.04 ± 0.48	**9.5 ± 0.24****	0.573 ± 0.688
	Control	9.4	8.27	0.074	9.13	7.87	0.055
27	Donor	10.17 ± 1.03	**9.9 ± 0.44***	1.068 ± 1.378	**10.27 ± 0.13*****	**9.94 ± 0.26*****	0.52 ± 0.275
	Control	10.19	8.65	0.029	9.26	7.95	0.049
43	Donor	10.26 ± 0.44	**10.25 ± 0.52***	2.98 ± 4.285	**10.37 ± 0.12*****	**9.94 ± 0.36****	0.432 ± 0.292
	Control	10.26	9.32	0.114	10.38	8.9	0.033
58	Donor	10.33 ± 0.49	**10.04 ± 0.31****	0.769 ± 0.84	9.64 ± 0.61	9.25 ± 0.48	0.564 ± 0.513
	Control	9.41	7.89	0.0301	9.43	7.68	0.018
72	Donor	**10.53 ± 0.18*****	**9.98 ± 0.38***	0.321 ± 0.167	10.42 ± 1.05	**9.77 ± 0.43***	0.386 ± 0.402
	Control	10.34	9.19	0.071	10.03	8.64	0.041
86	Donor	9.95 ± 0.74	**9.62 ± 0.35***	0.731 ± 0.811	8.73 ± 0.73	**8.52 ± 0.08****	1.208 ± 1.432
	Control	10.42	9.06	0.043	10.22	8.81	0.039
103	Donor	10.14 ± 0.48	**9.84 ± 0.41***	0.614 ± 0.504	9.47 ± 0.51	9.08 ± 0.46	0.846 ± 1.158
	Control	9.15	8.26	0.128	9.47	7.97	0.032
117	Donor	9.56 ± 0.22	9.41 ± 0.57	0.957 ± 0.83	9.71 ± 0.27	**9.38 ± 0.4***	0.542 ± 0.376
	Control	9.06	8.1	0.111	9.49	8.44	0.088
132	Donor	9.13 ± 0.54	8.73 ± 0.35	0.437 ± 0.22	9.74 ± 0.1	**9.63 ± 0.08*****	**0.796 ± 0.176***
	Control	9.18	8.23	0.113	9.77	8.78	0.101
150	Donor	9.34 ± 0.32	9.33 ± 0.58	1.114 ± 0.675	**8.98 ± 0.06*****	**8.78 ± 0.13***	0.651 ± 0.274
	Control	8.88	8.71	0.678	8.65	7.75	0.125
168	Donor	9.2 ± 0.37	9.27 ± 0.81	3.352 ± 4.89	**9.98 ± 0.24***	9.49 ± 0.58	0.686 ± 0.721
	Control	8.66	8.47	0.637	9.09	8.22	0.135
201	Donor	9.28 ± 0.65	9.23 ± 0.49	1.381 ± 1.307	**8.99 ± 0.08*****	**8.45 ± 0.07***	**0.293 ± 0.062***
	Control	8.33	8.17	0.7	9.02	8.11	0.124
254	Donor	9.58 ± 0.52	9.48 ± 0.88	1.638 ± 2.223	9.48 ± 0.51	9.28 ± 0.7	0.681 ± 0.329
	Control	8.79	8.04	0.176	9.12	7.89	0.059
303	Donor	9.37 ± 0.28	8.69 ± 0.08	0.247 ± 0.182	9.43 ± 0.65	**8.59 ± 0.17***	0.196 ± 0.136
	Control	9.17	8.43	0.18	8.43	7.68	0.176
340	Donor	9.41 ± 0.58	**8.8 ± 0.06****	0.385 ± 0.365	9.39 ± 0.23	**9.04 ± 0.19***	0.559 ± 0.474
	Control	9.22	8.04	0.065	8.93	7.64	0.051
357	Donor	9.57 ± 0.18	**9.97 ± 0.08*****	**2.605 ± 0.802***	9.15 ± 0.91	8.99 ± 0.64	0.828 ± 0.578
	Control	9.38	8.63	0.176	9.73	8.46	0.054
376	Donor	9.57 ± 0.09	**9.99 ± 0.12*****	2.818 ± 1.125	9.7 ± 1.09	**9.56 ± 0.53***	1.192 ± 1.04
	Control	9.36	8.94	0.377	10.39	8.76	0.024

Data for 16S gene copy numbers, ITS gene copy numbers, and the f:b ratio are shown for decomposition (donor) and control soils in both interface and core soil depths. Gene copy number data are represented as log copy number per gram dry weight of soils (gdw). Data are means ± standard deviations for $n = 3$ replicate donors and $n = 20$ controls (full study). Three outlier samples in which the f:b ratio exceeded 10 were removed. Impacted soils that significantly differ from full-study controls based upon Welch *t*-tests ($P < .05$) are presented in bold type. Data are means ± standard deviations for $n = 3$ replicate donors. Asterisks indicate levels of significance: *$P < .05$, **$P < .01$, and ***$P < .001$.

Table 8. Winter 2019 microbial abundances in interface (0–1 cm) and core (1–16 cm) soils.

Depth		Interface			Core		
Study day	Location	16S copy numbers (log copies gdw^{-1})	ITS copy numbers (log copies gdw^{-1})	Fungal:bacterial ratio	16S copy numbers (log copies gdw^{-1})	ITS copy numbers (log copies gdw^{-1})	Fungal:bacterial ratio
0	Donor	**10.7 ± 0.13****	**9.23 ± 0.16****	0.035 ± 0.011	**10.49 ± 0.06*****	**8.86 ± 0.07****	**0.024 ± 0.006***
	Control	10.58	9.25	0.046	10.33	8.7	0.024
21	Donor	**10.62 ± 0.08*****	8.94 ± 0.37	**0.024 ± 0.013***	10.27 ± 0.18	**8.89 ± 0.17***	0.044 ± 0.017
	Control	10.36	9.2	0.069	9.96	8.67	0.051
38	Donor	10.68 ± 0.29	7.46 ± 1.66	**0.009 ± 0.013****	10.33 ± 0.22	8.79 ± 0.38	0.035 ± 0.023
	Control	9.95	8.43	0.03	10.2	8.56	0.023
55	Donor	**10.91 ± 0.17****	**10.57 ± 0.73***	1.042 ± 1.173	10.31 ± 0.23	8.86 ± 0.64	0.045 ± 0.032
	Control	9.13	8.07	0.086	10.31	9.01	0.05
75	Donor	**10.57 ± 0.09*****	**10.14 ± 0.59***	0.566 ± 0.609	**10.51 ± 0.12****	**9.65 ± 0.16*****	0.149 ± 0.065
	Control	10.21	8.94	0.054	10.24	8.73	0.031
94	Donor	**10.99 ± 0.08*****	**10.01 ± 0.27*****	0.115 ± 0.059	**10.46 ± 0.16***	8.28 ± 0.61	**0.011 ± 0.012***
	Control	10.09	8.66	0.037	9.33	7.83	0.031
110	Donor	**10.67 ± 0.14****	**9.79 ± 0.3****	0.137 ± 0.047	10.28 ± 0.28	7.95 ± 1.5	0.027 ± 0.033
	Control	10.34	6.97	0.0004	10.4	8.32	0.008
126	Donor	10.79 ± 0.36	**9.81 ± 0.29****	0.112 ± 0.044	10.39 ± 0.18	9.5 ± 0.76	0.252 ± 0.315
	Control	10.45	9.17	0.053	10.51	8.25	0.005
140	Donor	**10.88 ± 0.19****	8.64 ± 1.22	0.026 ± 0.042	10.44 ± 0.43	8.93 ± 0.22	0.046 ± 0.051
	Control	10.31	8.99	0.049	10.14	8.37	0.017
158	Donor	10.79 ± 0.46	**9.5 ± 0.16*****	0.066 ± 0.059	10.22 ± 0.23	9.11 ± 0.4	0.083 ± 0.031
	Control	9.86	8.25	0.024	9.47	7.88	0.026
172	Donor	10.55 ± 0.25	**9.81 ± 0.42***	0.194 ± 0.078	10.34 ± 0.21	**9.48 ± 0.24****	0.196 ± 0.204
	Control	9.91	8.79	0.076	9.65	8.5	0.071
186	Donor	10.38 ± 0.29	**9.62 ± 0.36***	0.269 ± 0.206	10.14 ± 0.22	9.58 ± 0.61	0.395 ± 0.357
	Control	10.43	7.68	0.002	10.34	9.06	0.052
201	Donor	10.58 ± 0.63	**10.4 ± 0.49***	0.703 ± 0.284	9.82 ± 0.22	9.21 ± 0.81	0.395 ± 0.395
	Control	9.77	8.56	0.062	10.31	8.86	0.035
216	Donor	10.23 ± 0.24	9.34 ± 1.08	0.515 ± 0.519	10.01 ± 0.27	**9.43 ± 0.26***	0.304 ± 0.209
	Control	9.83	8.67	0.069	9.8	8.82	0.105
234	Donor	10.3 ± 0.12	**9.85 ± 0.17*****	0.378 ± 0.147	9.86 ± 0.27	**9.43 ± 0.33***	**0.375 ± 0.047****
	Control	10.21	8.73	0.033	9.72	8.47	0.056
252	Donor	9.97 ± 0.18	**9.64 ± 0.46***	0.544 ± 0.294	10.09 ± 0.24	9.32 ± 0.4	0.28 ± 0.322
	Control	9.71	8.72	0.102	9.84	8.29	0.028
290	Donor	**10.5 ± 0.03*****	**10.22 ± 0.16*****	0.553 ± 0.223	10.21 ± 0.14	**9.48 ± 0.25****	0.199 ± 0.096
	Control	10.42	9.46	0.109	10.06	8.67	0.04
335	Donor	**10.78 ± 0.08*****	**9.62 ± 0.27****	0.074 ± 0.029	10.15 ± 0.3	**9.42 ± 0.35***	0.277 ± 0.299
	Control	10.57	9.06	0.031	10.52	8.97	0.028
384	Donor	**10.64 ± 0.06*****	**9.81 ± 0.15*****	0.155 ± 0.056	**10.47 ± 0.06*****	**9.53 ± 0.09*****	**0.117 ± 0.034***
	Control	10.29	8.97	0.048	10.29	8.85	0.037

Data for 16S gene copy numbers, ITS gene copy numbers, and the f:b ratio are shown for decomposition (donor) and control soils in both interface and core soil depths. Gene copy number data are represented as log copy number per gram dry weight of soils (gdw). Data are means ± standard deviations for $n = 3$ replicate donors and $n = 19$ controls (full study). Impacted soils that significantly differ from full-study controls based upon Welch t-tests ($P < .05$) are presented in bold type. Data are means ± standard deviations for $n = 3$ replicate donors. Asterisks indicate levels of significance: *$P < .05$, **$P < .01$, and ***$P < .001$.

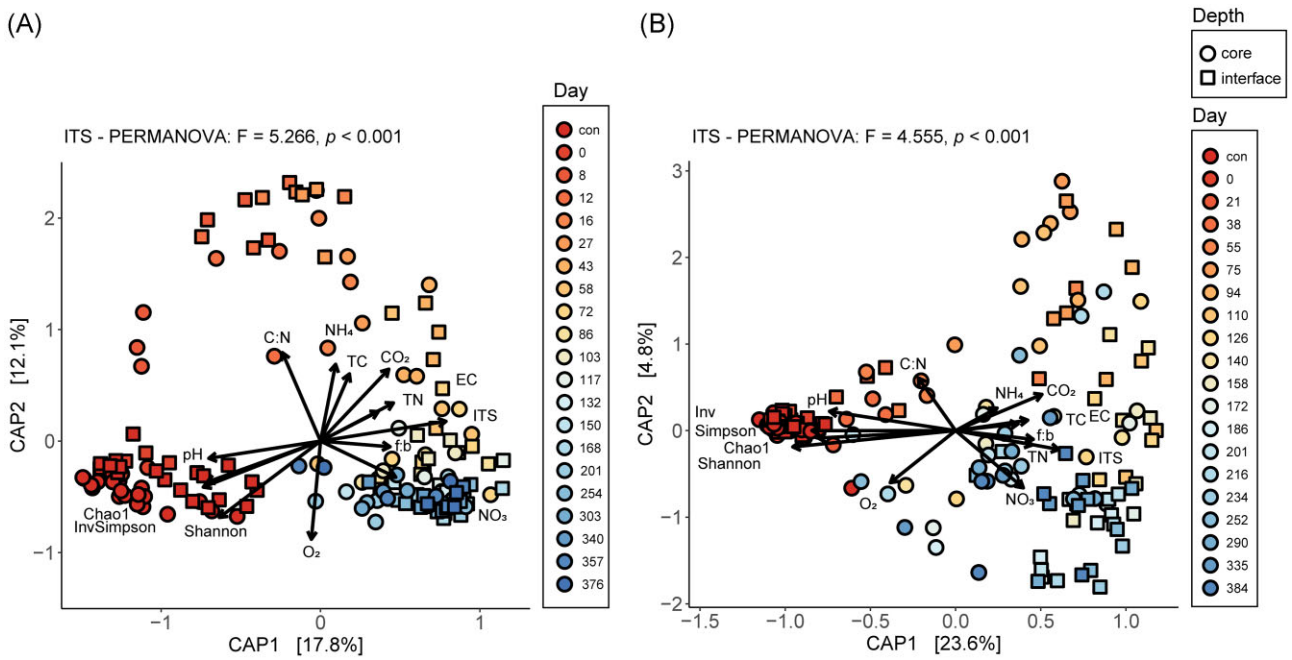

Figure 4. CAP coordinates ordination of fungal community structures. CAP plot of Bray–Curtis dissimilarities shows changes in fungal beta diversity between study days for both the (A) spring trial and (B) winter trial. Arrows show the influence of biogeochemical and biological variables: pH, EC, soil oxygen (O_2), respiration (CO_2), ammonium (NH_4), nitrate (NO_3), TC, TN, the carbon:nitrogen ratio (C:N), Shannon diversity, Inverse Simpson diversity (InvSimpson), Chao1 diversity, log ITS gene copy number (ITS), and the fungal:bacterial ratio (f:b). Winter trial communities exhibited greater dispersion. Community structure did not fully return to initial state after 1 year in either seasonal trial. Soil depth is indicated by shape: circles (1–16 cm cores) and squares (0–1 cm interfaces). Statistical differences between controls (con) and impacted soils were evaluated by PERMANOVA.

Gammoproteobacteria and *Actinobacteria*, and decreased *Verrucomicrobiae* and *Thermoleophilia*.

Winter 2019: bacterial community composition shifts during the winter trial were similar to those found in the spring trial in both soil depths, albeit at reduced magnitude and altered timing, similar to what we observed for fungal communities. *Firmicutes* were enriched in interfaces, but only up to 25% relative abundance, approximately half that observed in the spring trial, and were not accompanied by decreases in *Proteobacteria* (Supplementary file 1: Fig. S12). Relative abundances of *Bacteroidetes* increased slightly earlier in the winter trial, during active decay rather than early advanced decay as observed in the spring trial. At the class level, *Clostridia* briefly increased in impacted interface soils from days 75 to 94, commensurate with reduced pH, soil oxygen, and nitrate (Fig. 8; Supplementary file 1: Fig. S13). In winter interfaces both *Gammaproteobacteria* and *Bacteroidia* did not decrease with increases in *Clostridia*, but instead increased prior to increases in *Clostridia* by day 38, the onset of active decay. *Ignatzschineria* was observed on days 55 and 75, but only at <5% relative abundance (Supplementary file 2). Relative abundances of *Actinobacteria* increased in both soil depths during the *Clostridia* bloom and remained enriched for the remainder of the trial. *Verrucomicrobiae* and *Thermoleophilia* were not discernably impacted in core soils, however their abundances declined in interfaces during the *Clostridia* bloom and fell below detectable levels on days 126–172, as advanced decay transitioned to skeletonization.

Discussion

Our study was designed to evaluate the effects of surface-decomposition of whole human remains, incorporating simultaneously placed donors of similar mass, which were sampled at high resolution throughout a year. Our objectives were to characterize seasonal patterns in soil chemistry and microbial community abundance, diversity and structure at two soil depths, integrating the results in order to identify drivers of microbial change.

Seasonal differences in gross decomposition patterns

Morphological patterns of decomposition varied considerably between trials. The spring trial followed patterns frequently reported in the literature for warm-weather decomposition scenarios (Payne 1965, Carter et al. 2007, Meyer et al. 2013, Sutherland et al. 2013, Matuszewski et al. 2014, Suckling et al. 2016, Roberts et al. 2017, Connor et al. 2018, Dibner et al. 2019, DeBruyn et al. 2021): extensive bloating immediately followed by a brief period in which large amounts of decomposition fluids were quickly released into the soil, and an active decay period characterized by fly larval masses and rapid tissue loss. In this study, the period of advanced decay was prolonged (occurring in the winter) and skeletonization took place late in the trial as temperatures warmed. In contrast, winter trial decomposition patterns differed substantially: no insect masses were observed, minor scavenging was present in extremities, and donors exhibited negligible bloating with a more prolonged period of fluid seepage and tissue loss. In this instance, skeletonization occurred during the warm weather season, and earlier in general than observed in the spring trial. Vass et al. (1992) predicted skeletonization to occur at ~1285 ADD. We found that skeletonization occurred later in both trials: 4935 and 2682 ADD for the spring and winter trials, respectively.

Seasonal temperature patterns

Temperatures of decomposing vertebrate remains are frequently reported to increase up to 15°C above ambient temperatures in warm weather decomposition scenarios (Payne 1965,

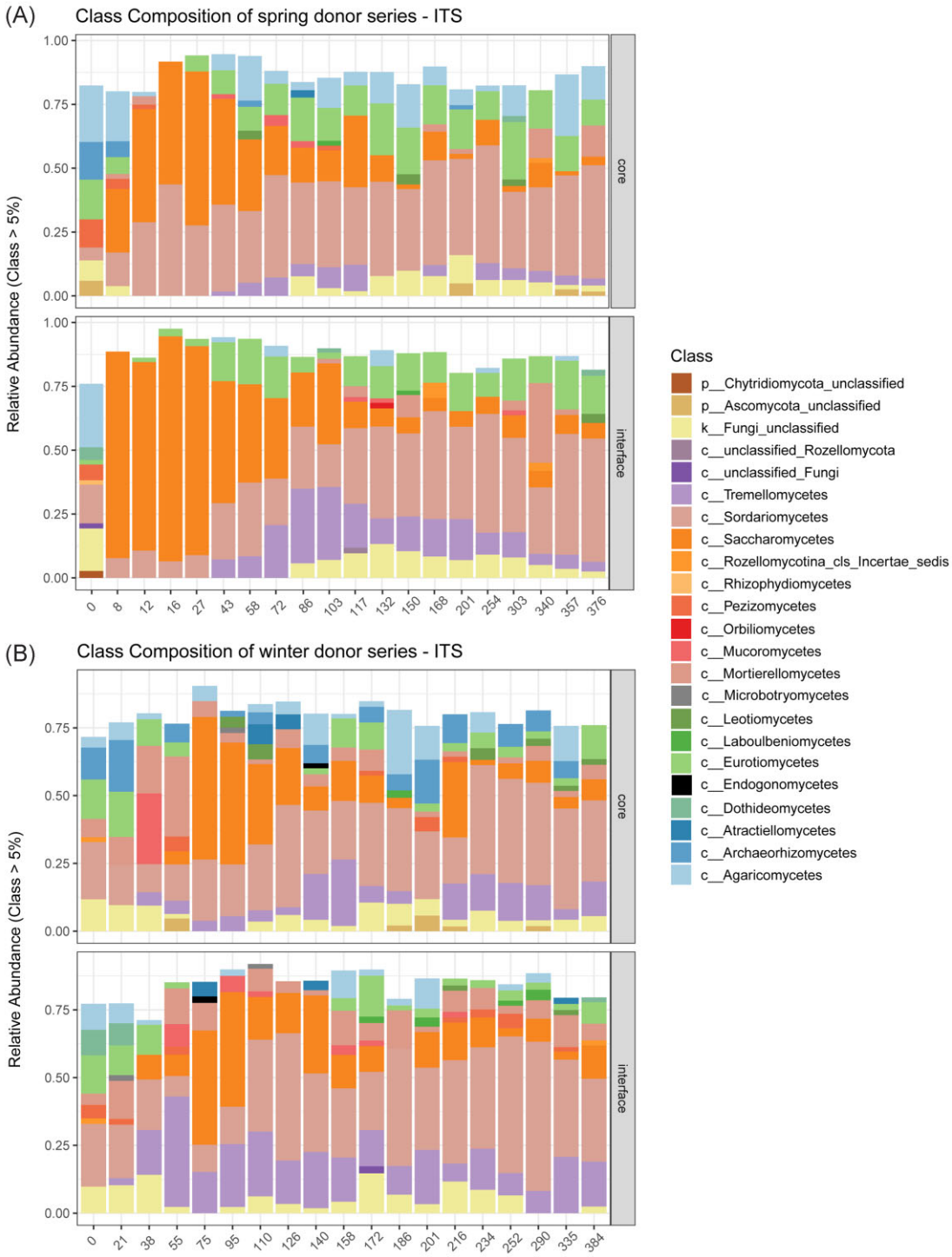

Figure 5. Soil fungal community composition during human decomposition. Relative abundances of fungal classes comprising >5% of communities in core (1–16 cm) and interface (0–1 cm) soils shown for the (A) spring and (B) winter trial.

Keenan et al. 2018b, Quaggiotto et al. 2019, Taylor et al. 2020, DeBruyn et al. 2021) and heat associated with larval masses (thermogenesis) is a well-known phenomenon (Heaton et al. 2014, Gruner et al. 2017, Weatherbee et al. 2017). The soil and internal donor heating results documented in our spring trial are consistent with previous reports for warm-weather decomposition in which larval masses were present (Payne 1965, Keenan et al. 2018b, Quaggiotto et al. 2019, Taylor et al. 2020, DeBruyn et al. 2021); internal and soil temperatures increased over those of ambient air and soil controls beginning during the bloat phase, and continued for 72 days into advanced decay, during which time temperatures exceeded 40°C, with at least 50 days >30°C. Conversely, soil and internal donor heating were absent from the winter trial, as were larval masses. These patterns support seasonal temperature patterns previously reported (DeBruyn et al. 2021).

Seasonal differences in temperature patterns have ramifications for data interpretation and PMI estimation. By the end of our spring study, cumulative ambient air temperatures had reached

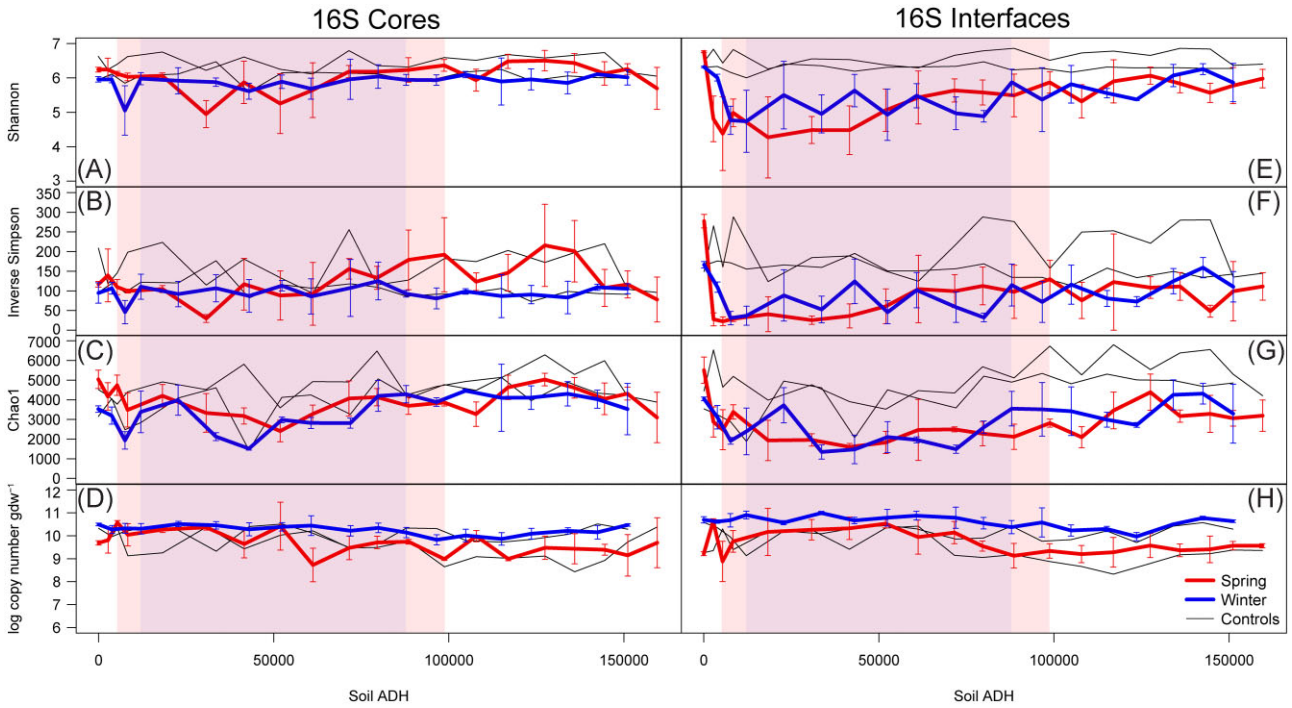

Figure 6. Seasonal comparisons in bacterial diversity in core and interface soils. The magnitude and timing of changes in (A and E) the Shannon index, (B and F) the Inverse Simpson index, (C and G) the Chao1 index, (D and H) and the log of gene copy number in core (1–16 cm) and interface (0–1 cm) soils are presented in units of equivalent thermal units based upon soil temperatures (soil ADH). Data is based on 16S sequences of bacterial rRNA genes, and abundance data was calculated based on bacterial gene copy numbers determined by qPCR. Means and standard deviations are shown for samples ($n = 3$). Controls for each time point were pooled. Shaded areas correspond to periods of reduced soil oxygen for the spring (light shading) and winter (darker shading).

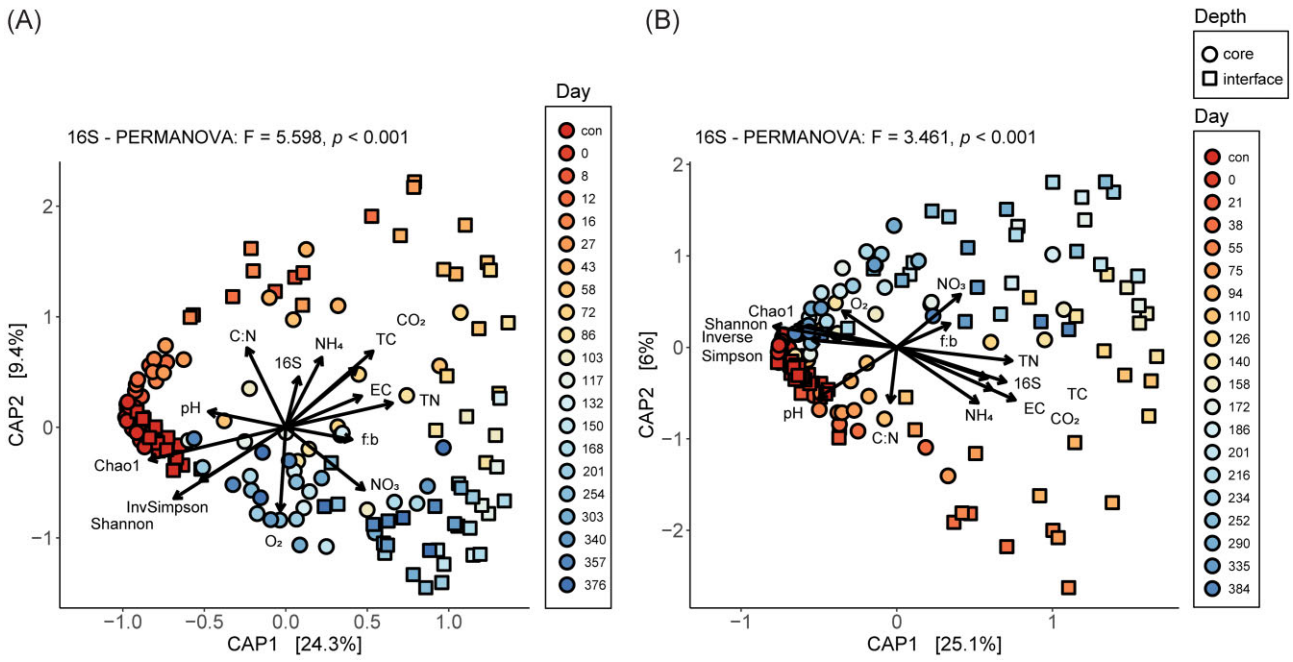

Figure 7. CAP coordinates ordination of bacterial community structures. CAP plot of Bray–Curtis dissimilarities shows changes in bacterial beta diversity between study days for both the (A) spring trial and (B) winter trial. Arrows show the influence of biogeochemical and biological variables: pH, EC, soil oxygen (O_2), respiration (CO_2), ammonium (NH_4), nitrate (NO_3), TC, TN, the carbon:nitrogen ratio (C:N), Shannon diversity, Inverse Simpson diversity (InvSimpson), Chao1 diversity, log 16S gene copy number (16S), and the fungal:bacterial ratio (f:b). Winter trial communities exhibited greater dispersion. Depth effects are evidenced by greater community dispersion in interface soils (0–1 cm). Soil depth is indicated by shape: circles (1–16 cm cores) and squares (0–1 cm interfaces). Statistical differences between controls (con) and impacted soils were evaluated by PERMANOVA.

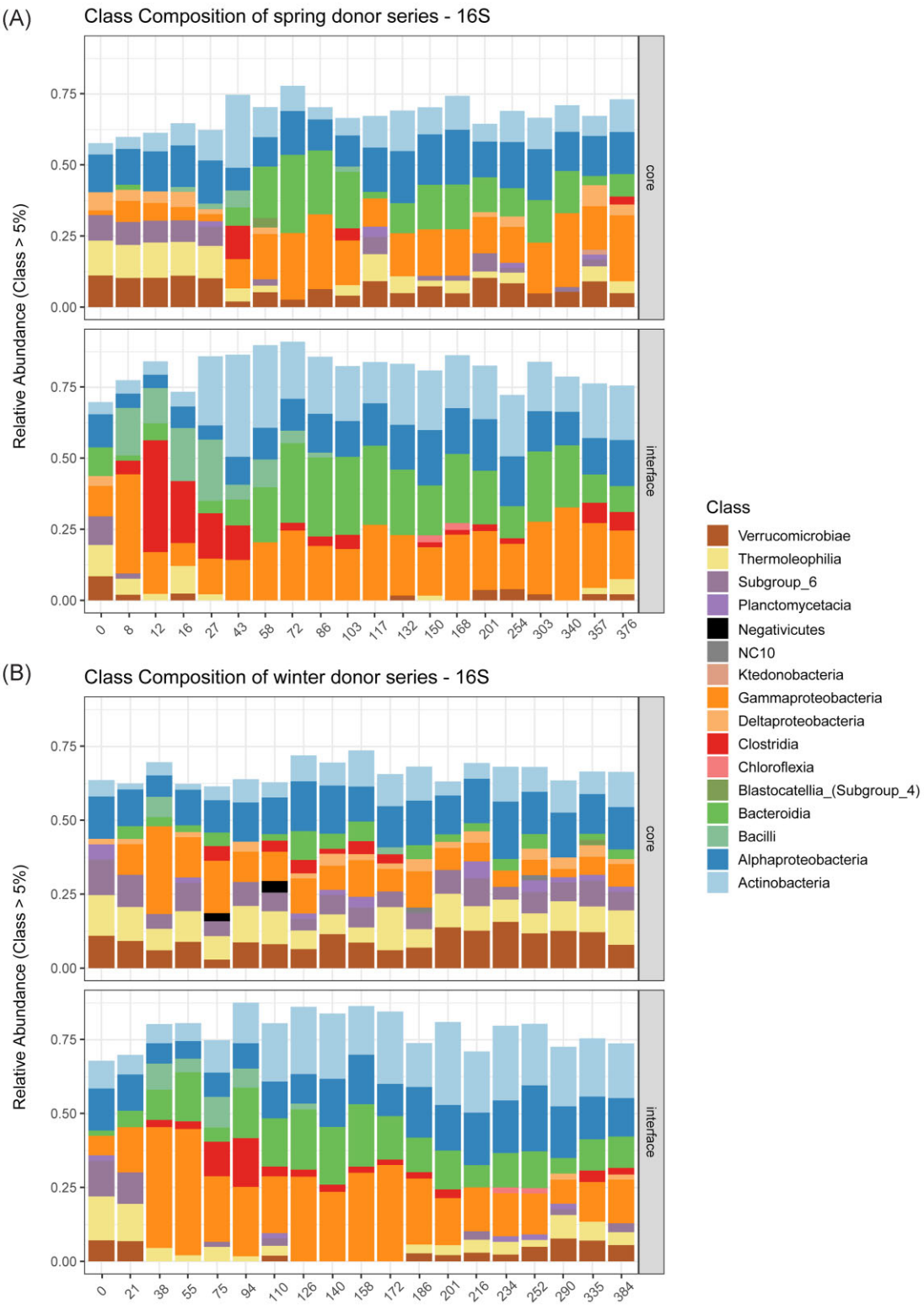

Figure 8. Soil bacterial community composition during human decomposition. Relative abundances of classes comprising >5% of communities in 1–16 cm cores and 0–1 cm interfaces for the (A) spring and (B) winter trials.

143 017 ADH, while cumulative internal and soil temperatures (in the presence of fly larvae, and thus larval thermogenesis) reached 156 039 ADH and 159 517 ADH, respectively, leading to a discrepancy of ~13 000–16 500 ADH after a year. Assuming that a typical East Tennessee summer day is roughly equivalent to 600 ADH, this would correspond to a 21.7–27.5-day (5.8%–7.3%) difference in PMI estimates depending on weather ambient or soil/internal temperatures were used. It is general practice in forensic study to use ambient air temperatures accessed from nearest-weather station data to calculate the ADD or ADH associated with

developmental stages of fly larvae, and from this information formulate estimates of the PMI. Temperature-dependent calculations (larval development, TBS:ADD relationships, and so on) and PMI estimates could be underrepresented by not accounting for localized heating effects (Dabbs 2010, 2015, Dourel et al. 2010, Hofer et al. 2020). Taken together, the extent of soil heating, particularly in conjunction with seasonality, may affect accuracy of both insect-based PMI estimations as well as other relationships based upon temperature (e.g. microbial metabolism and gene expression, soil enzyme activity rates, multicellular soil fauna reproduction strategies, and so on), and thus are knowledge gaps that warrant further exploration.

Seasonal soil chemistry patterns

In general, soil chemistry data from the spring trial followed patterns documented in the literature for aboveground decomposition, however the inclusion of a winter trial, high sampling resolution, and the long-term duration of our study was able to provide data leading to a more nuanced interpretation of previous material. Of all soil chemical parameters measured during decomposition, wide variability has been observed in response patterns of soil pH. Vertebrate (nonhuman) longitudinal surface-decomposition studies have generally shown pH to increase rather than decrease (Benninger et al. 2008, Metcalf et al. 2013, 2016, Meyer et al. 2013, Lauber et al. 2014, Macdonald et al. 2014, Szelecz et al. 2018, Keenan et al. 2018b, Quaggiotto et al. 2019) (but see Towne 2000, Anderson et al. 2013, Perrault and Forbes 2016). However, human surface longitudinal decomposition studies report that soil pH frequently (but not universally) decreased during decomposition (Vass et al. 1992, Cobaugh et al. 2015, DeBruyn et al. 2021, Mason et al. 2022, Taylor et al. 2023). In our study, soils acidified at a rate commensurate with the influx of decomposition products and remained impacted throughout the majority of both seasonal trials. Changes were more pronounced both in terms of time and magnitude in the spring study, (e.g. soil acidification occurred quickly and to a greater degree) and supported seasonal patterns reported by DeBruyn et al. (2021).

In both seasonal trials, patterns in soil TC reflected respiration rates, suggesting that considerable organic C is added to the soil during the early period of decomposition. This is consistent with reports of persistent soil C originating from sterols, long-chain aliphatic hydrocarbons, and their transformation products, which are derived from the decomposition of fats and tissue (Lühe et al. 2017, 2018). Additionally, TC in our study did not appear to translocate into deeper layers of the soil, further supporting similar reports by the same authors of decreased translocation of complex carbon structures. During decomposition, once the CDI had begun to "dry" we noted the formation of soil crusts that visibly appeared to contain adipocere, which would further retain carbon in the upper soil layers. Other vertebrate decomposition studies have shown inconsistent results in TC enrichment or depletion both during and following decomposition that cannot be explained by scavenging, seasonality, organism mass, sampling density, or time (Benninger et al. 2008, Parmenter and MacMahon 2009, Spicka et al. 2011, Anderson et al. 2013, Macdonald et al. 2014, Barton et al. 2016, Metcalf et al. 2016, Szelecz et al. 2018, Keenan et al. 2018b, Quaggiotto et al. 2019, Barton et al. 2020, Risch et al. 2020).

Increased respiration rates during active and advanced decay were coupled with significant reductions in soil oxygen concentrations in both seasonal trials; both parameters were less impacted in the winter trial due to the slower release of decomposition products into the soil than occurred in the spring. In both trials this period of hypoxia corresponded to increased relative abundance of facultative anaerobes including yeast (e.g. *Saccharomycetes*) and bacterial taxa (e.g. *Firmicutes*). The relative abundances of these organisms reflected seasonal magnitudes of respiration and soil oxygen (i.e. higher overall relative abundances of *Saccharomycetes* and *Firmicutes* in the spring trial). Other studies have also reported increases in anaerobic taxa during decomposition (Cobaugh et al. 2015, Metcalf et al. 2016, Adserias-Garriga et al. 2017, Singh et al. 2018, Mason et al. 2022). This period of reduced oxygen is important, because it constrains key biogeochemical transformations, particularly with respect to N cycling (Keenan et al. 2018b), and limits growth and activity of obligate aerobic decomposers. Despite its importance in constraining microbial metabolisms, soil oxygenation has only historically been discussed within the context of buried remains (Dent et al. 2004, Carter et al. 2007, 2008, 2010, Haslam and Tibbett 2009). In surface decomposition experiments, changes in soil oxygenation have only recently been directly measured (Keenan et al. 2018b).

Our study showed broadly sustained increases in TN due to decomposition, similar to prior results (Benninger et al. 2008, Parmenter and MacMahon 2009, Macdonald et al. 2014, Barton et al. 2016, 2020, Metcalf et al. 2016, Szelecz et al. 2018, Keenan et al. 2018b, Quaggiotto et al. 2019). As a result, at both soil depths, the C:N ratio fell below that of soil controls in the later phases of decomposition, indicative of continued N enrichment during and after C utilization. Early in decomposition, a pulse of ammonium is typical, resulting from breakdown of tissues by proteases from fly larvae and microbes (Meyer et al. 2013, Macdonald et al. 2014, Cobaugh et al. 2015, Metcalf et al. 2016, Szelecz et al. 2018, Keenan et al. 2018b, Quaggiotto et al. 2019, DeBruyn et al. 2021). In our study, the ammonium pulse was greater and occurred earlier in the spring trial compared to winter, similar to previous seasonal observations (DeBruyn et al. 2021). In all but winter core soils we observed nitrate concentrations in decomposition soils to decrease below controls during ammonium enrichment in the early phases of decay when soil oxygen dropped below ~75%. Once oxygen returned to 70%–75% later in decomposition, nitrate concentrations increased, indicating ammonium could be transformed via nitrification to nitrite and nitrate or nitrous oxide (Meyer et al. 2013, Macdonald et al. 2014, Metcalf et al. 2016, Szelecz et al. 2018, Keenan et al. 2018b). It is likely that other anaerobic nitrogen transformations were also occurring during the period of hypoxia [i.e. denitrification, dissimilatory nitrate reduction (DNRA), and annamox] as have been documented by other studies (Keenan et al. 2018b).

EC is directly related to the ionic strength of the soil and reflects collective changes in concentrations of K^+, Na^+, Ca^{2+}, Mg^{2+}, NH_4^+, and NO_3^- (Aitkenhead-Peterson et al. 2012, Perrault and Forbes 2016, Fancher et al. 2017, Lühe et al. 2017, Szelecz et al. 2018, Taylor et al. 2023). Our results showed that EC significantly increased during active decay in the spring trial and during advanced decay in the winter trial, consistent with what other studies have demonstrated (Aitkenhead-Peterson et al. 2012, Fancher et al. 2017, Keenan et al. 2018b, Quaggiotto et al. 2019, Mason et al. 2022, Taylor et al. 2023). It is interesting to note that EC peaks roughly align with peaks of both ammonium and nitrate. EC is the collective reflection of all cations and anions in the soil solution; increased quantities of elements soluble from the soil matrix under acidic conditions (notably Al^{3+}, Fe^{2+}, and Mn^{2+}) may also account for late study increases and overall persistence of EC in human decomposition (Taylor et al. 2023). Conversely, elemental insolubility under soil alkalinization, in combination with presumed impacts to EC may have interesting implications for

identifying limitations on the use of animals for modeling human decomposition patterns.

Seasonal microbial community patterns

In both seasonal trials, successional changes in fungal and bacterial community structures displayed three distinct phases that directly reflected changes in soil biogeochemistry, and correlated to soil oxygen and pH dynamics. A three-phase decomposition model was proposed by Keenan et al. (2018b) based upon biogeochemical changes documented under decomposing animals in a warm-weather study. Here, we validate that model and expand upon it by coupling these biogeochemical patterns with changes to both microbial community composition (relative abundance) and microbial gene copy number (absolute abundance).

Phase 1. From the beginning of the study through the onset of advanced decay microbial alpha diversity decreased, and community structure shifted. Peak relative abundances in *Saccharomycetes* (*Yarrowia*) and *Clostridia* were observed during this phase, with decreased *Verrucomicrobiae* and *Thermoleophilia*. Fungal abundances, estimated based on gene copies determined by qPCR increased, while bacterial abundances remained unchanged leading to an overall increase in the fungal:bacterial ratio. These microbial changes corresponded with decreases in pH, soil oxygen, and NO_3, and increases in EC, respiration, and NH_4. In the spring trial this first phase also included increased soil temperatures due to increased metabolic activity of microbes and insect larvae.

Phase 2. An inflection point in the trajectory of microbial community structure changes was observed around days 12–43 of the spring trial (ADD 257–967) and days 75–94 of the winter trial (ADD 822–1196) corresponding to soil oxygen minimums (39% and 71% DO for the spring and winter trials, respectively), and marked the beginning of a second phase of changes. This second phase occurred during the period of advanced decay and early skeletonization, in which soil oxygen gradually increased, respiration rates and NH_4 concentrations declined, and NO_3 increased with more readily available soil oxygen. Fungal alpha diversity and gene copy number during this second phase did not change appreciably, however bacterial alpha diversity increased slightly in interface communities in conjunction with soil oxygen increases. Both *Saccharomycetes* and *Clostridia* decreased in relative abundance, and *Sordariomycetes (Scedosporium)*, *Bacteroidia*, *Gammaproteobacteria*, and *Actinobacteria* began to increase.

Phase 3. Another inflection point was observed around days 132–168 of the spring trial (ADD 3131–3917) and days 172–186 of the winter trial (ADD 3021–3364) corresponding to soil oxygen recovery to >75% of initial levels, and the beginning of the third phase. This third phase included the period between late advanced decay through late skeletonization, when soil oxygen concentrations recovered to 100% and NO_3 remained elevated. Alpha diversity during this third phase continued to increase slowly in bacterial interface communities, slightly lagging behind oxygen recovery, accompanied by gradual reductions in *Bacteroidia* and increases in *Gammaproteobacteria* (spring only), *Verrucomicrobiae*, and *Thermoephila*. In conjunction with pH, fungal diversity remained low, but fungal gene abundances remained elevated. By the end of both trials (1 year later), fungal and bacterial community composition became more similar to initial structures but did not recover completely; the highest degree of recovery was evidenced in bacterial communities in winter core soils.

The changes in soil oxygen and pH during decomposition appear to be the primary drivers of microbial communities. Community structure changed and diversity decreased in response to the period of low soil oxygenation during active and advanced decomposition for both the spring and winter trials. This is likely due to a combination of activation of alternative anaerobic metabolic pathways and responses to anoxic stress. Further, the acidification of soil during decomposition is likely also playing a role in structuring microbial communities; pH is one of the primary determinants of soil microbial community structures (Fierer and Jackson 2006).

The increase in fungal, but not bacterial abundances was notable, and suggests that fungi are proliferating in decomposition soils. The lack of increase in bacterial abundances accompanying increased respiration suggest a decrease in carbon use efficiency which has been previously noted (Cobaugh et al. 2015) and is consistent with a switch to anaerobic metabolic pathways. Decreases in soil pH are often accompanied by an increase in fungi-to-bacteria ratios, generally attributed to the fact that fungi have greater tolerance for acidic conditions than many bacterial taxa (Rousk et al. 2009).

In both seasonal studies, the dominant members of the fungal community were two Ascomycetes: *Saccharomycetes* and *Sordariomycetes*. *Saccharomycetes* are monophyletic yeasts, most of which live as saprobes associated with a variety of ecological niches including soil, or in association with plants and animals (Suh et al. 2006). *Saccharomycetes* exhibited a brief bloom during bloat through advanced decay in the spring, and during early advanced decay in the winter study. Their growth may be explained by their ability to perform fermentation under anoxic conditions and a tolerance or preference for acidic conditions: *Saccharomyces cerevisiae* has been shown to achieve optimal growth in slightly acidic conditions (Ariño 2010, Peña et al. 2015). The presence of *Saccharomycetes* enrichment is consistent with other reports (Metcalf et al. 2013, 2016, Carter et al. 2015, Forger et al. 2019, Fu et al. 2019, Mason et al. 2022). The timing of increase in our study (3801 ambient ADH), as well as the presence of *Yarrowia* closely aligns with increases associated with spring donors in Mason et al. (2022) (3000–3500 ADH). Winter data from the same study showed some variability in the onset of *Saccharomycetes* enrichment (3000–11 500 ADH) and our results (22 782 ambient ADH), suggest that decomposition beginning in colder temperatures and/or climates in conjunction with the lack of insect activity may influence the timing associated with changes to abundant taxa. This further suggests that more study is required for cold-weather decomposition scenarios. The common soil saprobe *Sordariomycetes* (phylum Ascomycota) were the most prevalent taxa in fungal communities in later decomposition and remained highly enriched for the remainder of the study. This enrichment, particularly in the winter trial when tissue breakdown was slow, suggests that they thrive in nitrogen-rich, low pH environments. It is possible that *Sordariomycetes* might constitute members of "ammonia fungi" or "post-putrefaction fungi," which have been historically observed during decomposition (but not identified via DNA sequencing) (Sagara 1976, Tibbett and Carter 2003, Sagara et al. 2008). Alternatively, the presence of *Scedosporium aurantiacum* (Sordariomycetes) may have partially originated from decomposition products. *Scedosporium* spp. are commonly found in the environment and also serve as human pathogens, particularly in the immunocompromised (Kaur et al. 2019).

Relative abundances of the phylum *Basidiomycota* were reduced during active decomposition, but increased at later times. In the spring trial, *Tremellomycetes*, particularly orders *Trichosporonales* and *Agaricomycetes*, were enriched during mid-advanced decay concurrent with increases in soil nitrate; likewise, increases of both *Tremellomycetes* and nitrate occurred earlier in the winter

trial. Overall, this suggests that there might be a shift within *Basidiomycota* towards classes with an affinity for nitrate. These types of fungi have been previously identified as "late ammonia fungi" and are generally attributed to the appearance of fruiting structures 1–4 years following decomposition. Our DNA-based approach may have detected these taxa concurrent with elevated nitrate prior to the development of fruiting bodies and thus earlier than previously reported in the literature (Sagara 1976, Tibbett and Carter 2003, Sagara et al. 2008). Relative abundances of *Agaricomycetes* fluctuated in the winter trial in comparison with consistent relative abundances in controls, suggesting the possibility that decomposition products may be generally detrimental to these taxa. Other eukaryotic (18S rRNA) amplicon studies have noted the presence and potential value of *Agaricomycetes* to modeling the PMI but have not discussed changes to abundances (Metcalf et al. 2013, 2016, Carter et al. 2015).

Regarding bacterial community changes, both animal and human decomposition studies have shown consistent increases in *Firmicutes* relative abundances with decreases in *Acidobacteria* and *Verrucomicrobia* during active and early advanced decomposition; these changes are frequently accompanied with or followed by increases in *Bacteroidetes*, *Proteobacteria* and *Actinobacteria*. These population shifts are generally attributed to a combination of sudden increases in general nutrient availability, an influx of host microbes, and brief soil hypoxia (Metcalf et al. 2013, 2016, Lauber et al. 2014, Carter et al. 2015, Cobaugh et al. 2015, Adserias-Garriga et al. 2017, Singh et al. 2018, Mason et al. 2022).

In both seasonal trials we observed increased *Firmicutes* relative abundances beginning in bloat and active decay, which peaked at the onset of advanced decay in conjunction with high respiration rates, low soil oxygenation, and coinciding with the bloom of *Saccharomycetes* yeasts. The magnitude of this *Firmicutes* bloom was most apparent in the spring trial, and in interface soils, and diminished with soil reoxygenation. *Firmicutes* are opportunistic facultative anaerobes and likely have a competitive advantage during the period of hypoxia. At the class level, *Clostridia* appears to be the main taxon driving the *Firmicutes* blooms in both seasons; *Clostridia* is found in both vertebrate guts and soils and is commonly reported in early decomposition (Cobaugh et al. 2015, Metcalf et al. 2016, Adserias-Garriga et al. 2017, Mason et al. 2022).

Proteobacteria relative abundances were briefly reduced in the spring during increased relative abundances of *Firmicutes* and accompanying period of low soil oxygen, signifying that they were most likely responding to the greater magnitude of environmental changes present during warm-weather decomposition scenarios and/or were at a competitive disadvantage with *Firmicutes*. At the class level *Gammaproteobacteria*, and to a lesser extent *Alphaproteobacteria* exhibited increases immediately following the pronounced *Clostridia* bloom, and both taxa persisted throughout the spring trial. In contrast, both groups of taxa were enriched during the comparatively slight *Clostridia* bloom in the winter trial. Collectively these patterns support reports by Cobaugh et al. (2015) in which both *Gamma-* and *Alphaproteobacteria* increased as advanced decay progressed. *Proteobacteria* are broadly considered copiotrophic organisms, and typically respond strongly to increases in nutrient influx. Our observed decrease- then increase-patterns for these two groups of *Proteobacteria* are further suggestive that despite significant nutrient influx they are negatively affected by reduced oxygen, and that their later increases in relative abundance likely derive from continued soil impaction originating from long-term tissue degradation.

Bacteroidia demonstrated similar patterns of increase as observed with *Gammaproteobacteria*, however toward the end of both trials relative abundances began to decrease to initial levels. This suggests that moderate changes in soil oxygenation did not substantially impact these taxa, and that a favorable competitive window exists for these organisms following the decreases of *Clostridia*. Our results are in agreement with reports of *Bacteroides* found in later advanced decay and in anoxic grave soils containing remaining tissue (Cobaugh et al. 2015, Keenan et al. 2018a).

Study limitations

Human decomposition studies are subject to numerous constraints. Worldwide, there are only 12 facilities in which these types of studies can be performed, nine of which are located in the USA (Pesci et al. 2020); this serves to reduce the diversity of climate and soil types available for comparison and eliminate others altogether (but see Carter et al. 2023). Further, these facilities are reliant upon body donations, which in many cases restrict population metrics (age, sex, ancestry, and so on). Spatial constraints and land-use history at these facilities may dictate donor placement proximity and affect the availability of fresh soil, the latter potentially introducing the possibility of priming effects or enrichment in previously used areas (Damann et al. 2012). Human subjects are a rare resource, and donor availability in combination with facility physical constraints often serves to dictate sample size, which can be low, affecting statistical (and by extension, explanatory) power. Our study attempted to simultaneously address three issues endemic to human decomposition studies: the use of fresh soil, subjects of similar size, and simultaneous donor placement in the field. This necessitated a study size of $n = 3$ male donors per season. Frozen human subjects were used for this study, and the effect of freezing on decomposition products, decomposer communities, and their functions is currently unknown. Nonetheless, our biogeochemical and microbial results are commensurate with multiple published studies obtained by using both frozen and unfrozen cadavers/carcasses (Aitkenhead-Peterson et al. 2012, Metcalf et al. 2013, 2016, Lauber et al. 2014, Cobaugh et al. 2015, Fancher et al. 2017, Keenan et al. 2018b, Mason et al. 2023, and others found throughout the discussion.) Future studies should expand on cohort size and metrics, and include a wider variety of soil types and climates in order to ascertain whether the biogeochemical and microbial patterns reported here are robust.

Conclusions

In this pair of long-term seasonal trials, we have demonstrated that the changes in soil bacterial and fungal community structures are inexorably linked to changes in the physicochemical environment, and that these collective changes vary in magnitude by season. Our work reinforces the need to understand how abiotic filtering drives microbial successional patterns in these systems. The relationships we observed between soil chemistry and microbial succession further supports the biogeochemical model proposed by Keenan et al. (2018b) and suggests that the magnitudes and timings of fluctuations within soil chemical parameters may function as predictors for successional patterns in microbial communities. Increased fungal abundance, in combination with relatively static bacterial abundances, has potential for determining relative importance of taxon shifts for downstream microbial modeling efforts. Further, increased soil temperatures bolstered by larval thermogenesis in warm-weather decomposition systems suggest that thermal effects, specifically short-term heating, likely influence chemical and biological transformations

in the soil due to organismal thermal tolerances, enhanced extracellular enzymatic activity, and altered metabolic rates. Further studies in other systems (i.e. different climates, soils, plant communities, and so on) would be needed to assess the repeatability and robustness of our observed patterns. Given the strong abiotic filtering we observed, the move toward including microbial community assessments that focus more on function or activity (e.g. metatranscriptomics and metabolomics) may be more instructive when it comes to determining biological markers of decomposition.

Acknowledgements

The authors would like to thank the donors and their families, and the support of the University of Tennessee Forensic Anthropology Center personnel. We also thank S.W. Keenan, M. Starrett, V. Beard, M. White, and H. Cyr for their assistance in soil sampling and laboratory analyses. No living human subjects were involved, and therefore this study was exempt from review by the University of Tennessee Institutional Review Board. This manuscript is part of the Doctoral dissertation "A high resolution study of long-term vertebrate decomposition in human and animal model systems." Consent for use is granted by the author, Lois S. Taylor.

Author contributions

Lois S. Taylor (Conceptualization, Data curation, Formal analysis, Investigation, Methodology, Validation, Visualization, Writing – original draft, Writing – review & editing), Allison R. Mason (Investigation, Visualization, Writing – review & editing), Hannah L. Noel (Investigation, Writing – review & editing), Michael E. Essington (Methodology, Writing – review & editing), Mary C. Davis (Investigation, Writing – review & editing), Veronica A. Brown (Investigation, Methodology, Writing – review & editing), Dawnie W. Steadman (Resources, Writing – review & editing), and Jennifer M. DeBruyn (Conceptualization, Funding acquisition, Methodology, Project administration, Resources, Software, Supervision, Writing – review & editing)

Supplementary data

Supplementary data is available at *FEMSEC Journal* online.

Conflict of interest: None declared.

Funding

This work was supported by the National Institute of Justice (2017-R2-CX-0008 to L.S.T. and J.M.D.).

Data availability

Raw sequence reads are deposited in the NCBI Short Read Archive under BioProjects PRJNA1066312 (Spring data set) and PRJNA1070662 (Winter data set). Analysis files and R code are available at: https://github.com/jdebruyn/ARF-seasonal.

References

Abarenkov K, Zirk A, Piirmann T *et al.* Full mothur UNITE+INSD dataset 1. Version 04.02.2020. Mothur, 2020.

Adserias-Garriga J, Hernandez M, Quijada NM *et al.* Daily thanatomicrobiome changes in soil as an approach of postmortem interval estimation: an ecological perspective. *Forensic Sci Int* 2017;**278**:388–95. https://doi.org/10.1016/j.forsciint.2017.07.017.

Aitkenhead-Peterson JA, Owings CG, Alexander MB *et al.* Mapping the lateral extent of human cadaver decomposition with soil chemistry. *Forensic Sci Int* 2012;**216**:127–34. https://doi.org/10.1016/j.forsciint.2011.09.007.

Anderson B, Meyer J, Carter DO. Dynamics of ninhydrin-reactive nitrogen and pH in gravesoil during the extended postmortem interval. *J Forensic Sci* 2013;**58**:1348–52. https://doi.org/10.1111/1556-4029.12230.

Apprill A, McNally S, Parsons R *et al.* Minor revision to V4 region SSU rRNA 806R gene primer greatly increases detection of SAR11 bacterioplankton. *Aquat Microb Ecol* 2015;**75**:129–37. https://doi.org/10.3354/ame01753.

Ariño J. Integrative responses to high pH stress in *S.cerevisiae*. *Omics* 2010;**14**:517–23. https://doi.org/10.1089/omi.2010.0044.

Barton PS, McIntyre S, Evans MJ *et al.* Substantial long-term effects of carcass addition on soil and plants in a grassy eucalypt woodland. *Ecosphere* 2016;**7**. https://doi.org/10.1002/ecs2.1537.

Barton PS, Reboldi A, Dawson BM *et al.* Soil chemical markers distinguishing human and pig decomposition islands: a preliminary study. *Forensic Sci Med Pathol* 2020;**16:** 605–12. https://doi.org/10.1007/s12024-020-00297-2.

Benninger LA, Carter DO, Forbes SL. The biochemical alteration of soil beneath a decomposing carcass. *Forensic Sci Int* 2008;**180**:70–5. https://doi.org/10.1016/j.forsciint.2008.07.001.

Berry M. Microbial community diversity analysis tutorial with phyloseq. GitHub, 2016.

Burcham ZM, Weitzel MA, Hodges LD *et al.* A pilot study characterizing gravesoil bacterial communities a decade after swine decomposition. *Forensic Sci Int* 2021;**323**:110782. https://doi.org/10.1016/j.forsciint.2021.110782.

Carter DO, Metcalf JL, Bibat A *et al.* Seasonal variation of postmortem microbial communities. *Forensic Sci Med Pathol* 2015;**11**:202–7. https://doi.org/10.1007/s12024-015-9667-7.

Carter DO, Orimoto A, Gutierrez CA *et al.* A synthesis of carcass decomposition studies conducted at a tropical (Aw) taphonomy facility: 2013-2022. *Forensic Sci Int Synergy* 2023;**7**:100345. https://doi.org/10.1016/j.fsisyn.2023.100345.

Carter DO, Yellowlees D, Tibbett M. Cadaver decomposition in terrestrial ecosystems. *Naturwissenschaften* 2006;**94**:12–24. https://doi.org/10.1007/s00114-006-0159-1.

Carter DO, Yellowlees D, Tibbett M. Temperature affects microbial decomposition of cadavers (*Rattus rattus*) in contrasting soils. *Appl Soil Ecol* 2008;**40**:129–37. https://doi.org/10.1016/j.apsoil.2008.03.010.

Carter DO, Yellowlees D, Tibbett M. Moisture can be the dominant environmental parameter governing cadaver decomposition in soil. *Forensic Sci Int* 2010;**200**:60–6. https://doi.org/10.1016/j.forsciint.2010.03.031.

Cobaugh KL, Schaeffer SM, DeBruyn JM. Functional and structural succession of soil microbial communities below decomposing human cadavers. *PLoS One* 2015;**10**:e0130201. https://doi.org/10.1371/journal.pone.0130201.

Connor M, Baigent C, Hansen ES. Testing the use of pigs as human proxies in decomposition studies. *J Forensic Sci* 2018;**63**:1350–5. https://doi.org/10.1111/1556-4029.13727.

Cregger MA, Veach AM, Yang ZK *et al.* The *Populus* holobiont: dissecting the effects of plant niches and genotype on the microbiome. *Microbiome* 2018;**6**:31. https://doi.org/10.1186/s40168-018-0413-8.

Dabbs GR. Caution! All data are not created equal: the hazards of using National Weather Service data for calculating accumulated

degree days. *Forensic Sci Int* 2010;**202**:e49–52. https://doi.org/10.1016/j.forsciint.2010.02.024.

Dabbs GR. How should forensic anthropologists correct national weather service temperature data for use in estimating the postmortem interval?. *J Forensic Sci* 2015;**60**:581–7. https://doi.org/10.1111/1556-4029.12724.

Damann FE, Tanittaisong A, Carter DO. Potential carcass enrichment of the University of Tennessee Anthropology Research Facility: a baseline survey of edaphic features. *Forensic Sci Int* 2012;**222**:4–10. https://doi.org/10.1016/j.forsciint.2012.04.028.

Dautartas A, Kenyhercz MW, Vidoli GM *et al.* Differential decomposition among pig, rabbit, and human remains. *J Forensic Sci* 2018;**63**:1673–83. https://doi.org/10.1111/1556-4029.13784.

de Boer W, Folman LB, Summerbell RC *et al.* Living in a fungal world: impact of fungi on soil bacterial niche development. *FEMS Microbiol Rev* 2005;**29**:795–811. https://doi.org/10.1016/j.femsre.2004.11.005.

DeBruyn JM, Hoeland KM, Taylor LS *et al.* Comparative decomposition of humans and pigs: soil biogeochemistry, microbial activity and metabolomic profiles. *Front Microbiol* 2021;**11**:608856. https://doi.org/10.3389/fmicb.2020.608856.

Dent BB, Forbes SL, Stuart BH. Review of human decomposition processes in soil. *Environ Geol* 2004;**45**:576–85. https://doi.org/10.1007/s00254-003-0913-z.

Dibner H, Valdez CM, Carter DO. An experiment to characterize the decomposer community associated with carcasses (*Sus scrofa domesticus*) on Oahu, Hawaii. *J Forensic Sci* 2019;**64**:1412–20. https://doi.org/10.1111/1556-4029.14009.

Dourel L, Pasquerault T, Gaudry E *et al.* Using estimated on-site ambient temperature has uncertain benefit when estimating postmortem interval. *Psyche J Entomol* 2010;**2010**:1–7. https://doi.org/10.1155/2010/610639.

Fancher JP, Aitkenhead-Peterson JA, Farris T *et al.* An evaluation of soil chemistry in human cadaver decomposition islands: potential for estimating postmortem interval (PMI). *Forensic Sci Int* 2017;**279**:130–9. https://doi.org/10.1016/j.forsciint.2017.08.002.

Fierer N, Jackson RB. The diversity and biogeography of soil bacterial communities. *Proc Natl Acad Sci USA* 2006;**103**:626–31. https://doi.org/10.1073/pnas.0507535103.

Forger LV, Woolf MS, Simmons TL *et al.* A eukaryotic succession based method for postmortem interval (PMI) estimation of decomposing porcine remains. *Forensic Sci Int* 2019;**302**:109838. https://doi.org/10.1016/j.forsciint.2019.05.054.

Fu X, Guo J, Finkelbergs D *et al.* Fungal succession during mammalian cadaver decomposition and potential forensic implications. *Sci Rep* 2019;**9**:12907. https://doi.org/10.1038/s41598-019-49361-0.

Gruner SV, Slone DH, Capinera JL *et al.* Volume of larvae is the most important single predictor of mass temperatures in the forensically important Calliphorid, *Chrysomya megacephala* (Diptera: Calliphoridae). *J Med Entomol* 2017;**54**:30–4. https://doi.org/10.1093/jme/tjw139.

Hartgrove N. *Soil Survey of Knox County*. Nashville, TN: United States Department of Agriculture National Resources Conservation Service, 2006.

Haslam TCF, Tibbett M. Soils of contrasting pH affect the decomposition of buried mammalian (*Ovis aries*) skeletal muscle tissue. *J Forensic Sci* 2009;**54**:900–4. https://doi.org/10.1111/j.1556-4029.2009.01070.x.

Heaton V, Moffatt C, Simmons T. Quantifying the temperature of maggot masses and its relationship to decomposition. *J Forensic Sci* 2014;**59**:676–82. https://doi.org/10.1111/1556-4029.12396.

Hofer IMJ, Hart AJ, Martin-Vega D *et al.* Estimating crime scene temperatures from nearby meteorological station data. *Forensic Sci Int* 2020;**306**:110028. https://doi.org/10.1016/j.forsciint.2019.110028.

Kaur J, Kautto L, Penesyan A *et al.* Interactions of an emerging fungal pathogen *Scedosporium aurantiacum* with human lung epithelial cells. *Sci Rep* 2019;**9**:5035. https://doi.org/10.1038/s41598-019-41435-3.

Keenan SW, Emmons AL, Taylor LS *et al.* Spatial impacts of a multi-individual grave on microbial and microfaunal communities and soil biogeochemistry. *PLoS One* 2018a;**13**:e0208845. https://doi.org/10.1371/journal.pone.0208845.

Keenan SW, Schaeffer SM, DeBruyn JM. Spatial changes in soil stable isotopic composition in response to carrion decomposition. *Biogeosciences* 2019;**16**:3929–39. https://doi.org/10.5194/bg-16-3929-2019.

Keenan SW, Schaeffer SM, Jin VL *et al.* Mortality hotspots: nitrogen cycling in forest soils during vertebrate decomposition. *Soil Biol Biochem* 2018b;**121**:165–76. https://doi.org/10.1016/j.soilbio.2018.03.005.

Lauber CL, Metcalf JL, Keepers K *et al.* Vertebrate decomposition is accelerated by soil microbes. *Appl Environ Microbiol* 2014;**80**:4920–9. https://doi.org/10.1128/AEM.00957-14.

Lühe B, Birk JJ, Dawson L *et al.* Steroid fingerprints: efficient biomarkers of human decomposition fluids in soil. *Org Geochem* 2018;**124**:228–37. https://doi.org/10.1016/j.orggeochem.2018.07.016.

Lühe B, Fiedler S, Mayes RW *et al.* Temporal fatty acid profiles of human decomposition fluid in soil. *Org Geochem* 2017;**111**:26–33. https://doi.org/10.1016/j.orggeochem.2017.06.004.

Macdonald BCT, Farrell M, Tuomi S *et al.* Carrion decomposition causes large and lasting effects on soil amino acid and peptide flux. *Soil Biol Biochem* 2014;**69**:132–40. https://doi.org/10.1016/j.soilbio.2013.10.042.

Mason AR, McKee-Zech HS, Hoeland KM *et al.* Body mass index (BMI) impacts soil chemical and microbial response to human decomposition. *mSphere* 2022;**2022**:00325–22.

Mason AR, Taylor LS, DeBruyn JM. Microbial ecology of vertebrate decomposition in terrestrial ecosystems. *FEMS Microbiol Ecol* 2023;**99**:fiad006. https://doi.org/10.1093/femsec/fiad006.

Matuszewski S, Konwerski S, Fratczak K *et al.* Effect of body mass and clothing on decomposition of pig carcasses. *Int J Legal Med* 2014;**128**:1039–48. https://doi.org/10.1007/s00414-014-0965-5.

McMurdie PJ, Holmes S. phyloseq: an R package for reproducible interactive analysis and graphics of microbiome census data. *PLoS One* 2013;**8**:e61217. https://doi.org/10.1371/journal.pone.0061217.

Megyesi MS, Nawrocki SP, Haskell NH. Using accumulated degree-days to estimate the postmortem interval from decomposed human remains. *J Forensic Sci* 2005;**50**:1–9. https://doi.org/10.1520/JFS2004017.

Metcalf JL, Parfrey LW, Gonzalez A *et al.* A microbial clock provides an accurate estimate of the postmortem interval in a mouse model system. *eLife* 2013;**2**:19. https://doi.org/10.7554/eLife.01104.

Metcalf JL, Xu ZZ, Weiss S *et al.* Microbial community assembly and metabolic function during mammalian corpse decomposition. *Science* 2016;**351**:158–62. https://doi.org/10.1126/science.aad2646.

Meyer J, Anderson B, Carter DO. Seasonal variation of carcass decomposition and gravesoil chemistry in a cold (Dfa) climate. *J Forensic Sci* 2013;**58**:1175–82. https://doi.org/10.1111/1556-4029.12169.

Neuwirth E. *RColorBrewer Palettes*. ColorBrewer, 2014.

Notter SJ, Stuart BH, Rowe R *et al.* The initial changes of fat deposits during the decomposition of human and pig remains. *J Forensic Sci* 2009;**54**:195–201. https://doi.org/10.1111/j.1556-4029.2008.00911.x.

Oksanen J, Blanchet F, Friendly M *et al.* Vegan: community ecology package. CRAN, 2019.

Parada AE, Needham DM, Fuhrman JA. Every base matters: assessing small subunit rRNA primers for marine microbiomes with mock communities, time series and global field samples. *Environ Microbiol* 2016;**18**:1403–14. https://doi.org/10.1111/1462-2920.13023.

Parmenter RR, MacMahon JA. Carrion decomposition and nutrient cycling in a semiarid shrub-steppe ecosystem. *Ecol Monogr* 2009;**79**:637–61. https://doi.org/10.1890/08-0972.1.

Payne JA. A summer carrion study of the baby pig *Sus Scrofa* Linnaeus. *Ecology* 1965;**46**:592–602. https://doi.org/10.2307/1934999.

Peña A, Sánchez NS, Alvarez H *et al.* Effects of high medium pH on growth, metabolism and transport in *Saccharomyces cerevisiae*. *FEMS Yeast Res* 2015;**15**:fou005. https://doi.org/10.1093/femsyr/fou005.

Perrault KA, Forbes SL. Elemental analysis of soil and vegetation surrounding decomposing human analogues. *Can Soc Forensic Sci J* 2016;**49**:138–51. https://doi.org/10.1080/00085030.2016.1184840.

Pesci EL, Bronchti G, Crispino F *et al.* Perspectives on the establishment of a Canadian human taphonomic facility: the experiences of REST[ES]. *Forensic Sci Int Synerg* 2020;**2**:287–92.

Procopio N, Ghignone S, Voyron S *et al.* Soil fungal communities investigated by metabarcoding within simulated forensic burial contexts. *Front Microbiol* 2020;**11**:1686. https://doi.org/10.3389/fmicb.2020.01686.

Procopio N, Ghignone S, Williams A *et al.* Metabarcoding to investigate changes in soil microbial communities within forensic burial contexts. *Forensic Sci Int Genet* 2019;**39**:73–85. https://doi.org/10.1016/j.fsigen.2018.12.002.

Quaggiotto MM, Evans MJ, Higgins A *et al.* Dynamic soil nutrient and moisture changes under decomposing vertebrate carcasses. *Biogeochemistry* 2019;**146**:71–82. https://doi.org/10.1007/s10533-019-00611-3.

Quast C, Pruesse E, Yilmaz P *et al.* The SILVA ribosomal RNA gene database project: improved data processing and web-based tools. *Nucleic Acids Res* 2013;**41**:D590–6. https://doi.org/10.1093/nar/gks1219.

R Development Core Team. *R: A Language and Environment for Statistical Computing*. Vienna: R Foundation for Statistical Computing. 2010.

Rath KM, Fierer N, Murphy DV *et al.* Linking bacterial community composition to soil salinity along environmental gradients. *ISME J* 2019;**13**:836–46. https://doi.org/10.1038/s41396-018-0313-8.

Risch AC, Frossard A, Schuetz M *et al.* Effects of elk and bison carcasses on soil microbial communities and ecosystem functions in Yellowstone, USA. *Funct Ecol* 2020;**34**:1933–44. https://doi.org/10.1111/1365-2435.13611.

Roberts LG, Spencer JR, Dabbs GR. The effect of body mass on outdoor adult human decomposition. *J Forensic Sci* 2017;**62**:1145–50. https://doi.org/10.1111/1556-4029.13398.

Rousk J, Baath E, Brookes PC *et al.* Soil bacterial and fungal communities across a pH gradient in an arable soil. *ISME J* 2010;**4**:1340–51. https://doi.org/10.1038/ismej.2010.58.

Rousk J, Brookes PC, Bååth E. Contrasting soil pH effects on fungal and bacterial growth suggest functional redundancy in carbon mineralization. *Appl Environ Microbiol* 2009;**75**:1589–96. https://doi.org/10.1128/AEM.02775-08.

Sagara N. Presence of a buried mammalian carcass indicated by fungal fruiting bodies. *Nature* 1976;**262**:816. https://doi.org/10.1038/262816a0.

Sagara N, Yamanaka T, Tibbett M. Soil fungi associated with graves and latrines: toward a forensic mycology. In: *Soil Analysis in Forensic Taphonomy*. Boca Raton, FL: CRC Press, 2008, 67–107.

Schloss PD, Westcott SL, Ryabin T *et al.* Introducing mothur: open-source, platform-independent, community-supported software for describing and comparing microbial communities. *Appl Environ Microbiol* 2009;**75**:7537–41. https://doi.org/10.1128/AEM.01541-09.

Singh B, Minick KJ, Strickland MS *et al.* Temporal and spatial impact of human cadaver decomposition on soil bacterial and arthropod community structure and function. *Front Microbiol* 2018;**8**:12. https://doi.org/10.3389/fmicb.2017.02616.

Soil Survey Staff. *Soil Map*, Vol. **2018**. Nashville, TN: Natural Resources Conservation Service, United States Department of Agriculture, 2018.

Spicka A, Johnson R, Bushing J *et al.* Carcass mass can influence rate of decomposition and release of ninhydrin-reactive nitrogen into gravesoil. *Forensic Sci Int* 2011;**209**:80–5. https://doi.org/10.1016/j.forsciint.2011.01.002.

Steadman DW, Dautartas A, Kenyhercz MW *et al.* Differential scavenging among pig, rabbit, and human subjects. *J Forensic Sci* 2018;**63**:1684–91. https://doi.org/10.1111/1556-4029.13786.

Suckling JK, Spradley MK, Godde K. A longitudinal study on human outdoor decomposition in central texas. *J Forensic Sci* 2016;**61**:19–25. https://doi.org/10.1111/1556-4029.12892.

Suh SO, Blackwell M, Kurtzman CP *et al.* Phylogenetics of Saccharomycetales, the ascomycete yeasts. *Mycologia* 2006;**98**:1006–17. https://doi.org/10.1080/15572536.2006.11832629.

Sutherland A, Myburgh J, Steyn M *et al.* The effect of body size on the rate of decomposition in a temperate region of South Africa. *Forensic Sci Int* 2013;**231**:257–62. https://doi.org/10.1016/j.forsciint.2013.05.035.

Szelecz I, Koenig I, Seppey CVW *et al.* Soil chemistry changes beneath decomposing cadavers over a one-year period. *Forensic Sci Int* 2018;**286**:155–65. https://doi.org/10.1016/j.forsciint.2018.02.031.

Taylor LS, Gonzalez A, Essington ME *et al.* Soil elemental changes during human decomposition. *PLoS One* 2023;**18**:e0287094. https://doi.org/10.1371/journal.pone.0287094.

Taylor LS, Phillips G, Bernard EC *et al.* Soil nematode functional diversity, successional patterns, and indicator taxa associated with vertebrate decomposition hotspots. *PLoS One* 2020;**15:** e0241777. https://doi.org/10.1371/journal.pone.0241777.

Tibbett M, Carter DO. Mushrooms and taphonomy: the fungi that mark woodland graves. *Mycologist* 2003;**17**:20–4. https://doi.org/10.1017/S0269915X03001150.

Towne EG. Prairie vegetation and soil nutrient responses to ungulate carcasses. *Oecologia* 2000;**122**:232–9. https://doi.org/10.1007/PL00008851.

Vass AA, Bass WM, Wolt JD *et al.* Time since death determinations of human cadavers using soil solution. *J Forensic Sci* 1992;**37**:1236–53. https://doi.org/10.1520/JFS13311J.

Weatherbee CR, Pechal JL, Benbow ME. The dynamic maggot mass microbiome. *Ann Entomol Soc Am* 2017;**110**:45–53. https://doi.org/10.1093/aesa/saw088.

Weiss S, Carter DO, Metcalf JL *et al.* Carcass mass has little influence on the structure of gravesoil microbial communities. *Int J Legal Med* 2016;**130**:253–63. https://doi.org/10.1007/s00414-015-1206-2.

Wickham H. *ggplot2: elegant Graphics for Data Analysis*. New York, NY: Springer, 2016.

Wickham H. Easily install and load 'Tidyverse' packages. CRAN, 2017.

Received 9 March 2024; **revised** 8 July 2024; **accepted** 17 September 2024